

DTIC COPY

4

CONTRACTOR REPORT BRL-CR-628

BRL

LARGE BLAST AND THERMAL SIMULATOR REFLECTED WAVE ELIMINATOR STUDY

AD-A220 154

JAMES BUTZ
MOSHE KUNA
ROBERT L. GUICE
JAMES J. GOTTLIEB

MARCH 1990

DTIC
SELECTED
APR 6 1990
S B D
Co

APPROVED FOR PUBLIC RELEASE; DISTRIBUTION UNLIMITED.

U.S. ARMY LABORATORY COMMAND

BALLISTIC RESEARCH LABORATORY
ABERDEEN PROVING GROUND, MARYLAND

NOTICES

Destroy this report when it is no longer needed. DO NOT return it to the originator.

Additional copies of this report may be obtained from the National Technical Information Service, U.S. Department of Commerce, 5285 Port Royal Road, Springfield, VA 22161.

The findings of this report are not to be construed as an official Department of the Army position, unless so designated by other authorized documents.

The use of trade names or manufacturers' names in this report does not constitute indorsement of any commercial product.

UNCLASSIFIED

REPORT DOCUMENTATION PAGE			Form Approved OMB No. 0704-0188
Public reporting burden for this collection of information is estimated to average 1 hour per response, including the time for reviewing instructions, searching existing data sources, gathering and maintaining the data needed, and completing and reviewing the collection of information. Send comments regarding this burden estimate or any other aspect of this collection of information, including suggestions for reducing this burden, to Washington Headquarters Services, Directorate for Information Operations and Reports, 1215 Jefferson Davis Highway, Suite 1204, Arlington, VA 22202-4302, and to the Office of Management and Budget, Paperwork Reduction Project (0704-0188), Washington, DC 20503.			
1. AGENCY USE ONLY (Leave blank)	2. REPORT DATE March 1990	3. REPORT TYPE AND DATES COVERED Final, Sep 86 - Sep 87	
4. TITLE AND SUBTITLE Large Blast and Thermal Simulator Reflected Wave Eliminator Study		5. FUNDING NUMBERS PE: 62120 PR: AH25	
6. AUTHOR(S) James Butz, Moshe Kuna, Robert L. Guice, James J. Gottlieb			
7. PERFORMING ORGANIZATION NAME(S) AND ADDRESS(ES) Denver Research Institute University of Denver University Park Campus Denver, CO 80208		8. PERFORMING ORGANIZATION REPORT NUMBER	
9. SPONSORING / MONITORING AGENCY NAME(S) AND ADDRESS(ES) US Army Ballistic Research Laboratory ATTN: SLCBR-DD-T Aberdeen Proving Ground, MD 21005-5066		10. SPONSORING / MONITORING AGENCY REPORT NUMBER BRL-CR-628	
11. SUPPLEMENTARY NOTES			
12a. DISTRIBUTION / AVAILABILITY STATEMENT Approved for public release; distribution unlimited		12b. DISTRIBUTION CODE	
13. ABSTRACT (Maximum 200 words) <p>→ The design of a reflected wave eliminator (RWE) for the Large Blast/Thermal Simulator proposed by the U.S. Army was investigated. Activities were divided into two categories, theoretical and computer modeled analysis, and conceptual design of RWE candidate configurations. The design effort was concentrated on active RWEs where the open area changes over the time of the blast wave simulation. The computer analysis served to determine the rate of these area changes.</p> <p>Three different concepts were evaluated for the design of an active RWE. Stresses were analyzed and the power requirements to properly move the RWE during the passage of the blast wave were estimated. Two louver concepts were found to be of lighter weight and more easily moved than a radial fan concept. A rotating louver design was recommended for further study. In addition, vents in the side wall of the LB/TS near the RWE were recommended in order to provide the maximum open area needed. <i>key words</i></p>			
14. SUBJECT TERMS Large Blast/Thermal Simulator; Blast Wave Simulation; Rarefaction Wave Eliminator; Blast Wave Shaping; Shock Tube Flow; Wave Reflections; Comp. Fluid Dynamics. <i>(1/d)</i>		15. NUMBER OF PAGES	
17. SECURITY CLASSIFICATION OF REPORT UNCLASSIFIED		16. PRICE CODE 104	
18. SECURITY CLASSIFICATION OF THIS PAGE UNCLASSIFIED		19. SECURITY CLASSIFICATION OF ABSTRACT UNCLASSIFIED	
		20. LIMITATION OF ABSTRACT UL	

GENERAL INSTRUCTIONS FOR COMPLETING SF 298

The Report Documentation Page (RDP) is used in announcing and cataloging reports. It is important that this information be consistent with the rest of the report, particularly the cover and title page. Instructions for filling in each block of the form follow. It is important to stay *within the lines* to meet optical scanning requirements.

Block 1. Agency Use Only (Leave blank).

Block 2. Report Date. Full publication date including day, month, and year, if available (e.g. 1 Jan 88). Must cite at least the year.

Block 3. Type of Report and Dates Covered
State whether report is interim, final, etc. If applicable, enter inclusive report dates (e.g. 10 Jun 87 - 30 Jun 88).

Block 4. Title and Subtitle. A title is taken from the part of the report that provides the most meaningful and complete information. When a report is prepared in more than one volume, repeat the primary title, add volume number, and include subtitle for the specific volume. On classified documents enter the title classification in parentheses.

Block 5. Funding Numbers. To include contract and grant numbers; may include program element number(s), project number(s), task number(s), and work unit number(s). Use the following labels:

C - Contract	PR - Project
G - Grant	TA - Task
PE - Program Element	WU - Work Unit Accession No.

Block 6. Author(s) Name(s) Name(s) of person(s) responsible for writing the report, performing the research, or credited with the content of the report. If editor or compiler, this should follow the name(s).

Block 7. Performing Organization Name(s) and Address(es) Self-explanatory.

Block 8. Performing Organization Report Number. Enter the unique alphanumeric report number(s) assigned by the organization performing the report.

Block 9. Sponsoring/Monitoring Agency Name(s) and Address(es) Self-explanatory.

Block 10. Sponsoring/Monitoring Agency Report Number. (If known)

Block 11. Supplementary Notes. Enter information not included elsewhere such as: Prepared in cooperation with...; Trans. of...; To be published in... When a report is revised, include a statement whether the new report supersedes or supplements the older report.

Block 12a. Distribution/Availability Statement. Denotes public availability or limitations. Cite any availability to the public. Enter additional limitations or special markings in all capitals (e.g. NOFORN, REL, ITAR).

DOD - See DoDD 5230.24, "Distribution Statements on Technical Documents."

DOE - See authorities.

NASA - See Handbook NHB 2200.2.

NTIS - Leave blank.

Block 12b. Distribution Code.

DOD - Leave blank.

DOE - Enter DOE distribution categories from the Standard Distribution for Unclassified Scientific and Technical Reports.

NASA - Leave blank.

NTIS - Leave blank.

Block 13. Abstract. Include a brief (*Maximum 200 words*) factual summary of the most significant information contained in the report.

Block 14. Subject Terms. Keywords or phrases identifying major subjects in the report.

Block 15. Number of Pages. Enter the total number of pages.

Block 16. Price Code. Enter appropriate price code (*NTIS only*).

Blocks 17 - 19. Security Classifications. Self-explanatory. Enter U.S. Security Classification in accordance with U.S. Security Regulations (i.e., UNCLASSIFIED). If form contains classified information, stamp classification on the top and bottom of the page.

Block 20. Limitation of Abstract. This block must be completed to assign a limitation to the abstract. Enter either UL (unlimited) or SAR (same as report). An entry in this block is necessary if the abstract is to be limited. If blank, the abstract is assumed to be unlimited.

TABLE OF CONTENTS

	Page
1. Introduction	1
1.1 Previous Work	4
2. Objectives	7
2.1 Project Goal	7
2.2 Project Objectives	7
2.3 Procedure	8
3. Analytical and Numerical Approaches	9
3.1 Quasi-Steady Analysis	9
3.2 Unsteady Flow Analysis	17
3.3 Example Results of Quasi-Steady and Unsteady Analysis	17
4. Design Criteria	26
5. Active RWE Design Alternatives	27
5.1 Rotating Louvers	27
5.2 Hinged Louvers	46
5.3 Comparison of Hinged and Rotating Louver Concept . .	50
5.4 Stator-Rotor Concept	51
5.5 Side Venting	56
6. Conclusions and Recommendations	63
7. References	65
8. Appendix: Supplemental Side Venting Rarefaction Wave Eliminator	67



Accession For	
NTIS GRA&I	<input checked="" type="checkbox"/>
DTIC TAB	<input type="checkbox"/>
Unannounced	<input type="checkbox"/>
Justification _____	
By _____	
Distribution/ _____	
Availability Codes	
Dist	Avail and/or Special
A-1	

INTENTIONALLY LEFT BLANK.

LIST OF FIGURES

	Page
1. Possible Simulator Operational Envelope	2
2. Illustrations of an Incident Shock	10
3. Inflows Through the End and Side Vents of a Reflection Eliminator, Causing Head Losses Inside the Duct	14
4. Area Setting for a Reflection Eliminator With an End Vent Only Which Produces No Reflected Wave	18
5. Sensitivity of Reflection Eliminator Area Setting in Producing a Reflected Wave	20
6. Difference in Vent Areas from Using Either an End Vent or Side Vent in the Reflection Eliminator	20
7. Area Setting of an Active RWE with Sharp-Edged End Vents to Eliminate Reflections for the Case of a Decaying Simulated Blast Wave	22
8. Pressure and Flow Velocity Signatures for the Cases of an Infinite Duct Extension	24
9. LB/TS Rotating Louver Reflected Wave Eliminator Exit Plane	28
10. Three Views of Rotating Louver Concept Design	29
11. Front View of Rotating Louver Concept Design	30
12. Side View of Rotating Louver Concept Design	31
13. Top View of Rotating Louver Concept Design	32
14. LB/TS Reflected Wave Eliminator Comparative Rotating Louver's Cross Sections	33
15. LB/TS Hinged Louver Reflected Wave Eliminator Exit Plane	40
16. Three Views of Hinged Louver Concept Design	41
17. Front View of Hinged Louver Concept Design	42
18. Side View of Hinged Louver Concept Design	43
19. Top View of Hinged Louver Concept Design	44
20. Hinged Louver's Geometry and Analysis	45

21. LB/TS Reflected Wave Eliminator Stator Design	52
22. LB/TS Reflected Wave Eliminator Rotor Design	53
23. LB/TS Reflected Wave Eliminator Stator/Rotor Design . . .	54
24. Area Setting vs. Time for the Active Reflection Eliminator Used in the 13.8 kPa and Low-Yield Case . . .	57
25. Area Setting vs. Time for the Active Reflection Eliminator Used in the 103.3 kPa and Low-Yield Case . . .	58
26. Area Setting vs. Time for the Active Reflection Eliminator Used in the 241.2 kPa and Low-Yield Case . . .	59

LIST OF TABLES

	Page
1. Support Beams and Louvers for the LB/TS Reflected Wave Eliminator	35
2a. Power Requirements for One Rotating Louver for the 35-PSIG/10kT Case	37
2b. Power Requirements for One Optional Rotating Louver for the 35-PSIG/10 kT Case	37
3. Comparison Results Between Central Bar and Alternate Plate Louver Cross-Sections	39
4. Rotating Louver Aerodynamic Flutter Analysis Results . .	39
5. Force and Power Requirements for One Hinged Louver (with RW Jump) for the 35-PSIG/10 kT Case	49
6. Analysis Results for Hinged Louver Geometry, Weight and Maximum Power Requirements - for 100 Louvers	49
7. Hinged Louver Aerodynamic Flutter Analysis Results . . .	50
8. Comparison of Hinged and Rotating Louvers	50
9. LB/TS Exit Plane Open-Area Ratio Ranges for Stator/ Rotors Active RWE Designs.	55
10. Force and Power Requirements for One Hinged Louver (with Perfect Elimination of the Rarefaction Wave) for the 35-PSIG/10 kT Case	62

INTENTIONALLY LEFT BLANK.

PREFACE

The project reported here was conducted in support of an effort by the U.S. Army Ballistic Research Laboratory to define the systems and operational characteristics of a Large Blast and Thermal Simulator (LB/TS). The LB/TS would be a shock tube large enough to investigate the effects of battlefield blast and shock waves on full-scale military equipment. The successful implementation of a reflected wave eliminator on the LB/TS would significantly improve its performance and increase its cost effectiveness.

The Denver Research Institute would like to acknowledge the contribution of Mr. Richard Pearson, the contracting office's technical representative, in the guidance of this effort. Mr. Robert Guice of Applied Research Associates initiated this project while at DRI and has continued to be an integral member of the project team under subcontract. The modeling work and overall contribution of Prof. James J. Gottlieb and Ms. Kerry Scrase of the University of Toronto Institute for Aerospace Studies have been invaluable. Mr. Moshe Kuna, Research Associate on sabbatical at DRI, made the major contributions to the project, carrying out the conceptual designs of the RWE configurations based on theoretical/computer modeling analysis. Mr. Will Walters of DRI completed all of the concept design drawings on the CAD system, and DRI's Ms. Jackie Maddox edited this report.

INTENTIONALLY LEFT BLANK.

SUMMARY

The design of a reflected wave eliminator (RWE) for the Large Blast and Thermal Simulator (LB/TS) (a very large shock tube facility under consideration by the U.S. Army Ballistic Research Laboratory) was investigated. Activities were divided into two categories: theoretical/computer modeling analysis and conceptual design of RWE candidate configurations. The design efforts concentrated on active RWEs where the open area ratio changes over the time of the simulated blast wave. Such a design provides a more accurate simulation than a so-called passive RWE, but is more complicated to build and operate.

The computer analysis was performed with two different models. The simpler code is based on a steady or quasi-steady flow model and uses standard gas dynamics relations governing one-dimensional steady flow through a convergent nozzle and nonstandard relations from two-dimensional flows (Chaplygin's theory) to include jet contraction effects, in order to calculate the actual area reduction required of the RWE for a given strength of the incident shock wave (flat-topped). By preselecting the proper area constriction of the RWE, the flow can be tuned such that no reflected waves from the RWE, outside of a short transient spike, are produced to readjust the flow to the RWE area setting. In the case of a decaying blast wave with time, this steady flow analysis can be used as a quasi-steady flow analysis to estimate the proper area reduction of the RWE at each new time as the flow conditions change. The steady flow analysis cannot predict transient flow effects. For predicting transient flows, a fully unsteady one-dimensional computer code with two-dimensional jet contraction effects was developed. This much more sophisticated code is called the random-choice method or model (RCM). With the RCM the transient spike can be predicted if the RWE area setting is correctly set, and the reflected waves produced by an RWE area mis-setting can be predicted and assessed.

The initial theoretical evaluation was done with the quasi-steady model because of its ease of use and ability to provide information

rapidly over a wide range of input conditions. This analysis quickly indicated the significant advantage of an active RWE over a passive system. This advantage was confirmed in the more rigorous analysis provided by the RCM.

Three different configurations were evaluated for the conceptual design of an active RWE. Two employed slat-type louvers (venetian blinds) on a framework at the end of the LB/TS, each with a different approach to the way the open area ratio is changed; while the third used a radial fan that rotated about an axis parallel to the direction of flow in the LB/TS. Calculations were made for the stresses to be encountered by the designs as well as for the power requirements to properly position the RWE elements to minimize reflected waves from the end of the LB/TS. The louver concepts were found to be both lighter in weight and more easily moved than the radial fan design. Because of the short time interval of the blast wave simulation (less than 300 milliseconds positive phase duration for a 10 kT, 241 kPa shock), the RWE requires power on the order of 1491 kilowatts for proper operation.

A rotating louver design was recommended for further investigation, including testing on a small scale shock tube to evaluate its performance experimentally. In addition, the use of RWE vents in the side wall of the LB/TS was also recommended to provide for the maximum total open area ratio predicted by the computer models.

1.0 INTRODUCTION

The Ballistic Research Laboratory is currently conducting research on various concepts to create a Large Blast and Thermal Simulator (LB/TS). This facility would actually be the world's largest shock tube, in which military systems and civil defense structures could be tested on a full or nearly full size scale. During this current research phase many different devices and subsystems are under study to determine their operating parameters and feasibility for incorporation into the LB/TS system.

In order for the LB/TS to be useful for various system test requirements, it must generate shockwaves that simulate a variety of blast conditions. Figure 1 shows a possible operational envelope of peak static pressure (associated with various yields of interest) and their respective positive phase durations. The shock wave properties which must be adjusted to cover the range defined in the operational envelope are the pressure amplitude and time duration. The amplitude of the shock wave can be adjusted by varying the initial driver conditions. The duration cannot be adjusted as easily.

An important consideration in the design of most shock tubes and blast wave simulators is either the avoidance or minimization of the reflected wave from the tube end beyond the test section. This reflected wave is a shock if the end is closed and a rarefaction wave when it is open. As this wave travels upstream towards the test section it alters the late time characteristics of the primary shock wave. For example, the pressure is reduced and flow velocity increased in the case of a reflected rarefaction wave, while the opposite is true for a reflected shock. This primary wave alteration extends into the test section if the duct length between the test section and tube end is short and the wave duration is long, thereby disrupting the desired flow environment or flow simulation in the test section.

The simple method of extending the duct beyond the test section to prevent the reflected wave from disturbing the desired test-section

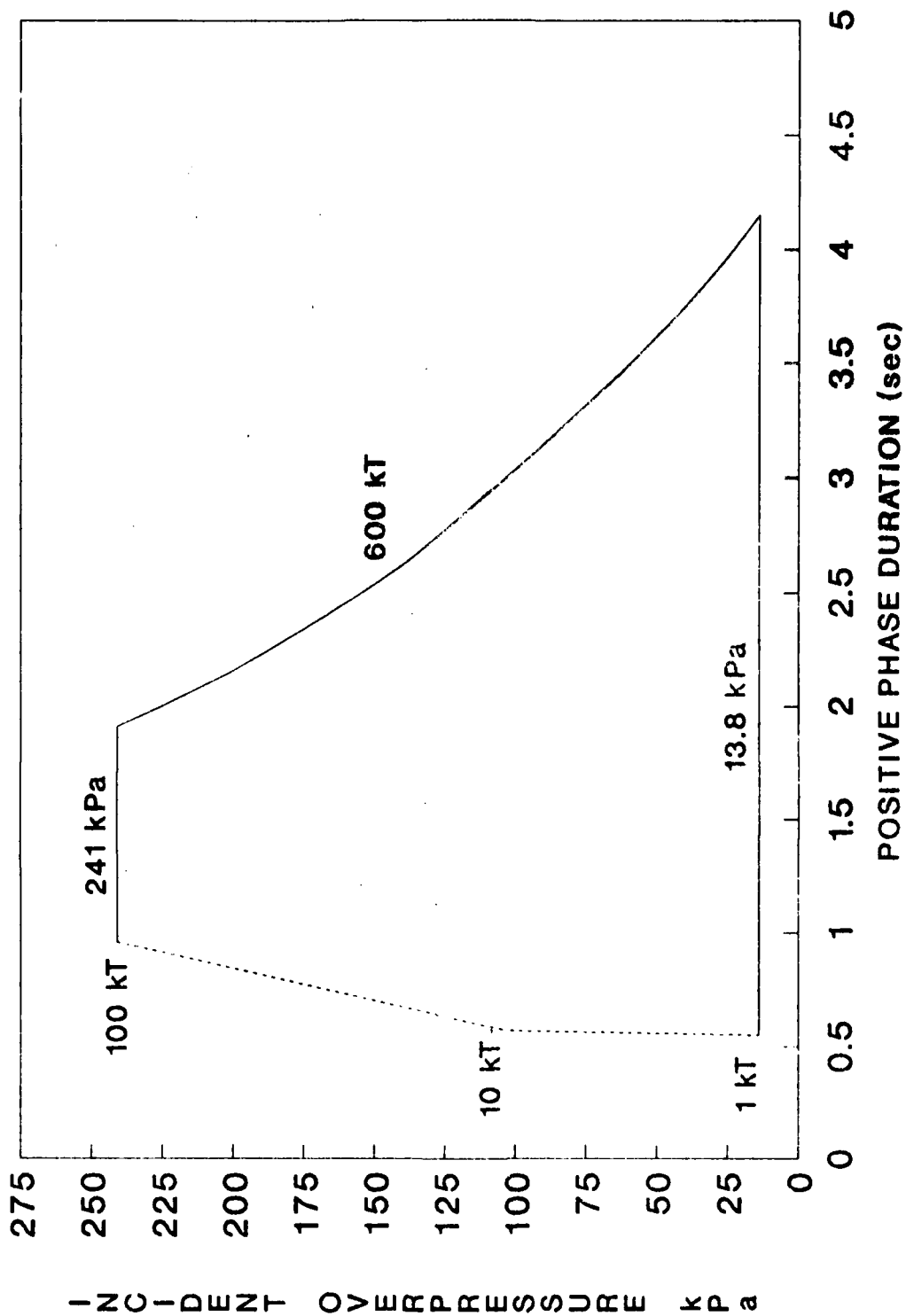


Figure 1 Possible simulator operator's envelope.

environment does not eliminate the reflected wave. Instead it delays the passage of this wave through the test section until after the test is complete. The required length of extra duct depends on the strength of the shock at the front of the blast wave and on the decay rate and duration of the wave. Longer duration waves obviously require longer tube extensions. The use of a sufficiently long tube extension will avoid all test-section disturbances during the testing time. Hence, this is the ideal approach from a performance viewpoint. For many small shock and blast tubes the installation of additional duct length is not much of a financial and space burden; however, when the tube diameter is large the cost and space requirements can become exorbitant.

Another method of minimizing the disturbing effect of the reflected wave at the test section is to use a short length of duct terminated by a reflection or rarefaction wave eliminator (RWE). An RWE is a device that partly covers the open tube end and as the blast wave leaves the duct end it basically produces a converging nozzle flow with a jet extending into the surrounding atmosphere. This jet can be entirely subsonic with its pressure matched to that of the atmosphere or choked with a pressure higher than the atmospheric value, depending on the incident shock stagnation pressure. In either case, a selection of the proper RWE flow blockage or area reduction can minimize the amplitude of the reflected expansion wave which would otherwise move upstream into the oncoming subsonic flow from the incident blast wave. If this disturbance is small from an RWE, then the need for any long and costly tube extension for large facilities is simply alleviated. The degree of success of any RWE, however, depends partly on its design and mostly on whether it is passive, semi-active or fully active.

A passive RWE has a constant area opening (or blockage) that is preset for a specific type and amplitude of incident shock or blast wave, and a semi-active RWE has a preprogrammed open area variation with time for a certain expected shock or blast wave. Although a fully active RWE has never been used, its area variation with time would not be preprogrammed, but instead flow sensors and feedback would be used to automatically update the area opening with time to weaken the reflected

disturbance. A fully active RWE would need to be properly controlled by preprogrammed algorithms having the ability to quickly analyze sensor data and make good, real time judgments as to the correct area setting to minimize the reflection.

For larger shock tubes and blast simulators (for which the cost of a tube extension becomes exorbitant in contrast to short extensions terminated by an RWE), a passive RWE is less costly than an active one, but an active RWE will perform better in weakening the reflection from the tube end. Because the quality of blast simulation has become more important today, test-section disturbances from reflected waves are now less acceptable. Consequently, to conduct higher quality blast testing of military equipment, active reflection elimination is becoming a necessity for large blast simulators.

The Denver Research Institute (DRI), Applied Research Associates of Denver (ARA), and the University of Toronto's Institute for Aerospace Studies (UTIAS) have been working together for the U.S. Army Ballistic Research Laboratory to study RWEs for the Large Blast Thermal Simulators. This effort was divided into two main categories: analytical/numerical modeling and the conceptual design of RWEs for the large blast simulator.

1.1 PREVIOUS WORK

The first documented efforts to use RWE concepts occurred in the 1950s by Niblett¹, Dosanjh², Weidemann³, Franks⁴ and Rudinger⁵. Their RWEs were all passive, since the shock tube open end was covered by a wire grid or screen, a plate with single or multiple holes, or a plate with a peripheral gap or stand-off distance from the end. Rudinger⁵ also experimented with porous, energy absorbing materials at the duct end in an attempt to remove a commonly observed overshoot on the reflected wave from an RWE (transient reflected spike). These early experiments were instrumental in establishing feasibility in weakening the reflected wave.

The use of passive RWEs on blast wave simulators began in the late 1950s and continues to the present time. Work was also done by Sadwin and Berman⁶ on RWEs for conical blast simulators, but an actual device was not built for any large facility. Some blast simulators of modest size (2 m diameter) used a flat plate with standoff RWEs mounted on tracked wheels to permit the blast impulse to move them away from the tube end, in order to circumvent the need for a massive stationary foundation to hold them at a fixed standoff distance. One such RWE is at the Prins Maurits Laboratory in Holland.⁷ Most blast simulators in United States, France, Germany, England, Switzerland, Holland, Canada, Norway, and Sweden were or are equipped with passive RWEs, but only the largest is mentioned here. At the Atomic Weapons Research Establishment (Foulness, England) the passive RWE was a stationary wall with a fixed standoff of 1.4 m from the 4.9 m diameter tube,⁸ but this has recently been changed to a stationary grill of horizontal bars without standoff,⁹ which now covers an extended and enlarged half-cylinder end 5.35 m high. Occasionally a foam plug is placed ahead of the grill, which can help reduce the overshoot noted by Rudinger⁶ in the 1950s.

From the early 1970s to the present there has been a growing emphasis on using active RWEs, especially on large blast simulators to obtain improved performance in contrast to that for passive RWEs. However, only two semi-active RWEs have been used, and both are at the Centre d'Etudes de Gramat. Each RWE consists of horizontal louvers which are preprogrammed to rotate to alter the vented area at the tube end. The smallest is employed on a modest size 2.4 m diameter shock tube¹⁰, and the largest is installed on a large blast simulator with a half-cylinder about 7 m high.¹¹

Recently in the mid 1980s the U.S. Army Ballistic Research Laboratory undertook some interesting and intensive experimental studies of different passive RWEs.^{12,13} The initial study¹² was done with a small 5.08 cm diameter shock tube and RWEs consisting of (1) a solid reflecting plate with a variable standoff distance from the open end, (2) a plate having one or more vent holes with and without a standoff distance, and (3) a grill of horizontal spaced bars with and without a

standoff distance. Their subsequent extended study¹³ with the same shock tube investigated additional RWE concepts summarized below.

flat plate	(without standoff, with/without foam)
vented plate	(with/without standoff, with/without foam)
bar grill	(single and multiple grills, with standoff)
needle bundle	(spaced out bundle of solid, pointed rods inside the tube end and facing upstream)
pipe bundle	(spaced out bundle of beveled front pipes inside the tube end and facing upstream)
parallel slats	(spaced out horizontal and parallel sharp-edged slats like knife blades facing into the flow)
steel wool	(steel wool placed ahead of a flat plate with vents and standoff distance)

Their tests showed that the vented plate with foam and the multiple grill of iron bars were the most promising. Some of these passive RWEs were also tested on a larger 0.57 m diameter shock tube, and a flat-plate RWE with standoff was tested on a even larger 2.44 m diameter shock tube, in order to prove that RWEs can be scaled from small to larger shock tubes and blast simulators.

2.0 OBJECTIVES

2.1 PROJECT GOAL

For unsteady shock tube flows, it is well known that the overpressure history of a shock wave can be dramatically affected by interaction caused by the open end of the shock tube, downstream from the test section. In order to simulate blast waves over a range of interest with a shock tube of limited length, some method of rarefaction wave control is required. This project investigated the feasibility of several different techniques for the elimination of rarefaction waves generated by an open end in the LB/TS. These investigations included both active and passive concepts, which were modeled with a computer program. An engineering analysis was also conducted to accumulate information on the predicted performance and requirements for the candidate techniques. The final product is a set of recommended configurations for a further detailed design and subsequent scaled fabrication and testing.

2.2 PROJECT OBJECTIVES

The effort outlined above has been divided into several phases to facilitate the evaluation of concepts and to provide decision points at which results can be examined and the scope of the study can be focused on candidate concepts which provide the most promising solution for the RWE problem. The work is guided by a series of objectives that define the purview and constraints under which the investigation is to be conducted. These are summarized as follows:

- o To develop and evaluate several concepts for active or passive RWEs for the LB/TS;
- o To recommend one or more active or passive RWE designs for use in the LB/TS;

- o To prepare relative cost estimates for the active or passive designs;

- o To develop, accumulate, organize and present supporting materials for the selection of an RWE concept for implementation on the LB/TS. This information will include details of the technical design, performance and relative costs for the candidate concepts.

2.3 PROCEDURE

Most of this study has concentrated on the active RWE concepts, since the literature surveyed indicated that existing information addresses to a greater extent the design and performance of passive RWEs. The first goal was to develop several concepts for active RWEs, that would be evaluated for use on the LB/TS. As an evaluation tool, a computer model of an RWE in a flow field was developed at UTIAS. Results from this model were combined with other analyses such as: 1) stresses applied to the candidate designs by the shock wave, 2) calculation of power requirements for motion of the RWE designs during the passage of the shock wave, and 3) initial design of the structural support required for the RWE.

3.0 ANALYTICAL AND NUMERICAL APPROACHES

Theoretical studies can be beneficial in identifying relevant designs of passive and active RWEs for shock tubes and blast simulators, as well as in doing parametric studies to help select optimum design parameters. Two complementary approaches are outlined here and example results given. The first approach is a quasi-steady analysis for determining the RWE area setting which produces virtually no reflection, or a reflected wave of specified amplitude, where the incident wave can be either a flat-topped shock or a decaying blast wave. Because the quasi-steady analysis does not include most transient wave phenomena, the second approach is a full, unsteady one-dimensional flow analysis with two-dimensional effects of friction, heat transfer, heat losses from grills, and mass losses from side vents corrected into the one-dimensional analysis via mass averaging (across the flow). The two approaches are not given in detail, but some relevant parts are presented and discussed.

3.1 QUASI-STEADY ANALYSIS

Consider a flat-topped shock or decaying blast wave which is moving in a duct of constant area A_0 , as shown in Figure 2a. It will interact with the RWE having a end vent area A_e and side vent area S_e . After this interaction there will be a reflected wave moving upstream and free jets issuing from the vents, as shown in Figure 2b. The reflected wave with a short transient spike or overshoot will be either a shock or an expansion wave when the combined vent areas are too small or too large, respectively, or it will be only a spike if the combined vent areas are set correctly, as illustrated in Figure 2c.

For an incident shock wave with a specified shock Mach number M_S , the pressure p_2 , flow velocity u_2 and sound speed a_2 behind this shock are given by

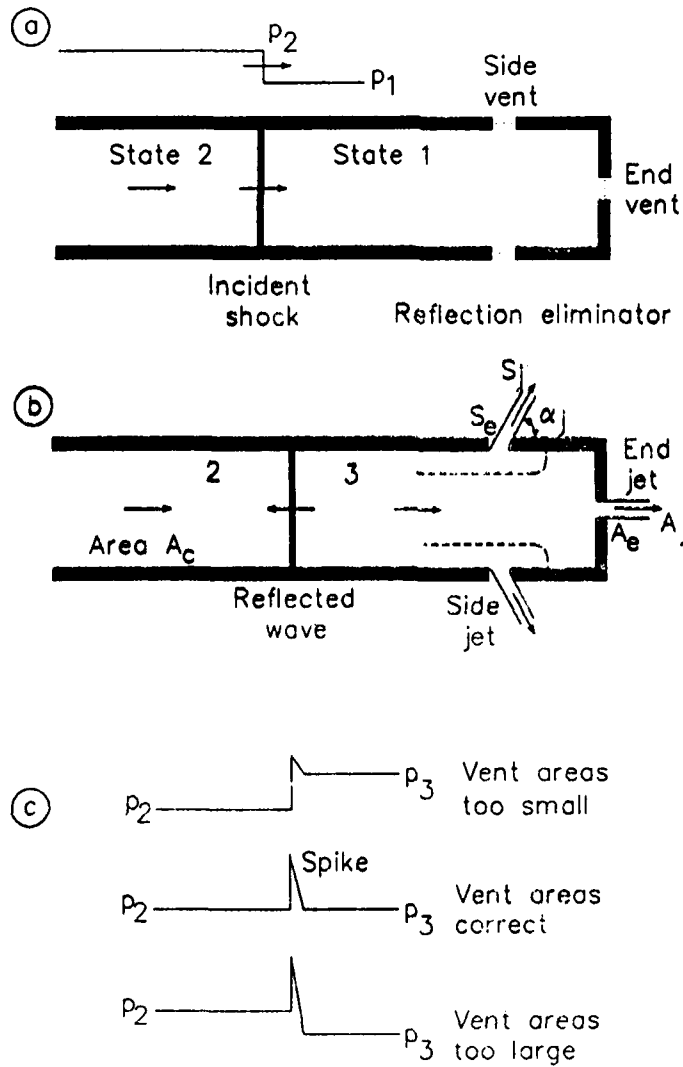


Figure 2. Illustrations of an incident shock approaching a reflection eliminator with side and end vents (a), subsequent reflected wave and side and end free jets (b), and reflected wave with a leading spike for vents set too small, correct and too large (c).

$$p_2 = p_1 \left[1 + \frac{2\gamma}{\gamma+1} (M_s^2 - 1) \right], \quad (1)$$

$$u_2 = \frac{2}{\gamma+1} a_1 (M_s - 1/M_s), \quad (2)$$

$$a_2 = a_1 \left[(\alpha + p_2/p_1) / (\alpha + p_1/p_2) \right]^{1/2}, \quad (3)$$

where $\alpha = (\gamma+1)/(\gamma-1)$ and the subscript 1 denotes atmospheric conditions ahead of the incident shock and outside the duct. In the specific case when the combined vent areas are set correctly, state 3 on the other side of the spike is then given by $p_3 = p_2$, $u_3 = u_2$ and $a_3 = a_2$. If the reflection is a shock wave of specified or guessed amplitude ($p_3/p_2 > 1$), then state 3 is given by

$$M_s = \left[1 + \frac{\gamma+1}{2\gamma} p_3/p_2 - 1 \right]^{1/2}, \quad (4)$$

$$u_3 = u_2 + \frac{2}{\gamma+1} a_2 (M_s - 1/M_s), \quad (5)$$

$$a_3 = a_2 \left[(\alpha + p_3/p_2) / (\alpha + p_2/p_3) \right]^{1/2}. \quad (6)$$

Finally, if the reflection is a rarefaction wave with a specified or guessed amplitude ($p_3/p_2 < 1$), then

$$u_3 = u_2 + \frac{2}{\gamma-1} a_2 \left[1 - (p_3/p_2)^{(\gamma-1)/2\gamma} \right], \quad (7)$$

$$a_3 = a_2 (p_3/p_2)^{(\gamma-1)/2\gamma}, \quad (8)$$

define the flow velocity and sound speed in state 3.

The compressible flow from state 3 through the end and side vents to the atmosphere is assumed isentropic. Furthermore, the flow properties in the two free jets are identical, because the same gas and same stagnation pressure in state 3 drives both free jets. In this case the isentropic equation

$$p_3 = p_j \left[\frac{2 + (\gamma-1)M_j^2}{2 + (\gamma-1)M_3^2} \right]^{\gamma/(\gamma-1)} = p_j [W_3/W_j]^{\gamma/(\gamma-1)} \quad (9)$$

relates the knowns p_3 and M_3 to the unknowns p_j and M_j for both jets, where M is the flow Mach number (u/a) and W denotes $2/[2 + (\gamma-1)M^2]$. For subsonic jets the jet pressure p_j is equal to atmospheric pressure p_1 , and Eq. 9 permits a direct calculation of the jet Mach number M_j .

For choked or sonic jets M_j is equal to unity. The free jet flows are subsonic if p_1 exceeds a critical jet pressure obtained from Eq. 9 with $M_j = 1$; otherwise the two jets are choked.

The application of continuity of mass in the main duct of area A_c , free jet of area A_j and side free jet of area S_j yields

$$A_j + S_j = A_c [M_3/M_j] [W_3/W_j]^{\alpha/2}. \quad (10)$$

At this point in the analysis, it is convenient to introduce state 4 just ahead of the end vent, because the mass flow at this point must leave through the end jet. Although the stagnation properties in states 3 and 4 are the same, the static flow properties and the mass and momentum fluxes are different, owing to the mass and momentum losses through the side jets. The solution of the properties in state 4 depends on state 3 and the properties of the free jets, and this complicates the solution procedure. Applying both conservation of mass and momentum from state 3 to state 4 gives

$$S_j = A_c \frac{M_3 W_3^{\alpha/2} - M_4 W_4^{\alpha/2}}{M_j W_j^{\alpha/2}}, \quad (11)$$

and

$$\cos(\alpha_j) = \frac{1}{YM_j W_j^{1/2}} \frac{(1 + YM_3^2) W_3^{Y/(Y-1)} - (1 + YM_4^2) W_4^{Y/(Y-1)}}{M_3 W_3^{\alpha/2} - M_4 W_4^{\alpha/2}} \quad (12)$$

These three equations have four unknowns: A_j , S_j , M_4 and the side jet angle α_j . If A_j , S_j , or A_j/S_j is specified or guessed, then the others can be determined.

The areas A_j and S_j are normally smaller than the actual vent openings given by A_e and S_e respectively, because these free jets generally contract on leaving the vents, unless the vent opening edges are well rounded. Also, S_j is the area normal to its jet stream, and in addition to the contraction the side jet angle α_j is needed before S_e can be obtained. A_e and A_j are related by the equation $A_j = C_e A_e$, where C_e is the contraction coefficient of the end jet, and S_e and S_j are

related by $S_j = S_e C_s \sin(\alpha_j)$, where C_s is the corresponding contraction coefficient of the side jet.

The contraction coefficient for the free jet from an end vent with sharp edges can be determined from theory.¹⁴ Although the results are in the form of an ill-conditioned hypergeometric series, tabulated values have been used with curve fits for easy reproduction. The final results are summarized below:

$$\tau_4 = (\gamma-1)M_4^2/[2 + (\gamma-1)M_4^2], \quad \tau_j = (\gamma-1)M_j^2/[2 + (\gamma-1)M_j^2], \quad (13)$$

$$\xi_j = \tau_j/(1 - \tau_j), \quad C_\infty = \pi/[\pi + 2 - 5\xi_j + 2\xi_j^2], \quad (14)$$

$$\eta = 7\tau_j + 1/(1+12\tau_j), \quad A = (2\eta-1)(1-C_\infty), \quad B = 2(1-\eta)(1-C_0), \quad (15)$$

$$C_0 = C_\infty + A(\tau_4/\tau_j) + B(\tau_4/\tau_j)^2, \quad (16)$$

where C_0 is the contraction coefficient for sharp-edged vents, and C_∞ is the contraction coefficient for the case of compressible jet flows through an orifice when the upstream area A_0 is infinitely larger than A_e .

If the end vent edges are not perfectly sharp but rounded instead, then a correction must be applied to C_0 from Eq. 16. The empirical correction used here is $C_e = C_0 + \omega(1-C_0)$, where ω ranges from zero for sharp edges to unity for rounded edges. From experiments at the UTIAS, $\omega = 1 - \exp(-90R_0/D_h)$, where R_0 is the radius of rounding of the vent edges and D_h is the hydraulic diameter of the vent opening. By using C_∞ , C_0 , ω and C_e , therefore, one can finally get $A_e = A_j/C_e$.

For the side vent we have a similar analysis: $S_e = S_j/(C_s \sin\{\alpha_j\})$, where $C_s = C_0 + \omega(1-C_0)$, $\omega = 1 - \exp(-90R_0/D_h)$, and C_0 is given by Eqs. 13 to 16, but with M_4 replaced by M_3 .

Although the previous analysis for outflows is algebraic, the nonlinear interdependence of the unknowns makes the solution procedure iterative in all but the simplest of problems. One primary complication is introduced by the contraction coefficients (which have been ignored

in all previous work). For example, if the knowns were the incident shock strength p_2/p_1 and the actual areas A_e and S_e , the solution procedure might be to first guess the strength p_3/p_2 of the reflected wave to determine the flow properties in state 3, such that the jet flow properties can be calculated (mainly M_j). Then one might guess a value of M_4 and iterate until the proper values of A_j , C_e and A_e are obtained. Once this is done, S_j , C_e and S_e are computed. If this S_e is not equal to the specified value, then one must choose an improved value of p_3/p_2 and repeat the process until the computed and specified values of S_e agree.

In the case of blast waves with negative phases, the sub-ambient pressure and reversed flow velocity result in inflow from the atmosphere into the blast simulator. Although reflection elimination for this negative phase has been entirely overlooked in the past, an active RWE can also be used here. The quasi-steady analysis for inflows is now given, which will allow one to determine the vent area settings which produce minimal reflections for this case. The flow properties in state 2 are assumed known as a function of time, from a decaying blast signature.

The flow properties in state 3 are the same as in state 2, because a proper area setting of the end and side vents should eliminate the reflected wave. The inflows of atmospheric air will produce a contact surface, as shown in Figure 3.

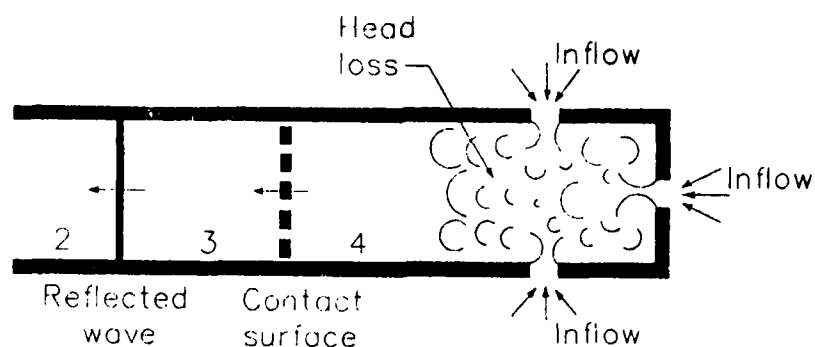


Figure 3 Inflows through the end and side vents of a reflection eliminator, causing head losses inside the duct.

In state 4 just behind this contact surface one can set $u_4 = u_3$ and $p_4 = p_3$. To obtain the remainder of the flow properties in state 4, note that the inflows from the atmosphere are basically adiabatic, even if friction, upstream-facing shocks and expansion flow losses occur. In this case the steady-flow energy equation with no heat transfer is

$$a_4^2 + \frac{\gamma-1}{2} u_4^2 = a_1^2, \quad (17)$$

where a_1 is the atmospheric speed of sound. This equation then yields a_4 , and $\rho_4 = \gamma p_4 / a_4^2$ and the mass flow rate is given by $\rho_4 A_c u_4$.

By assuming that the inflows from the atmosphere to the minimum area of the contracted flows are isentropic, the following expression

$$p_j / p_1 = (\rho_j / \rho_1)^\gamma = (a_j / a_1)^{(\gamma-1)/2\gamma} = \left[1 + \frac{\gamma-1}{2} M_j^2\right]^{-\gamma/(\gamma-1)} \quad (18)$$

relates the flow properties of the jets to the atmosphere. If the jet inflows are subsonic, the pressure p_j is approximately equal to the duct pressure just inside the RWE. In this case, a pressure drop occurs in the flow direction from the vent openings to state 4. This drop is given by

$$P_j - p_4 = k[\rho_j u_j^2 / 2] = k[\gamma p_j M_j^2 / 2], \quad (19)$$

where k is the head-loss coefficient. This coefficient depends on the area expansion from the combined jet flow area $A_j + S_j$ to the duct area A_c , according to

$$k = [1 - (A_j + S_j) / A_c]^2, \quad (20)$$

which varies from a minimum of zero when $A_j + S_j = A_c$ to a maximum of unity when $A_j + S_j$ is much smaller than A_c . The combined jet area $A_j + S_j$ is given by

$$A_j + S_j = \frac{\rho_4 A_c u_4}{\rho_j a_j M_j} = \frac{\rho_4 A_c u_4}{\rho_1 a_1 M_j} \left[1 + \frac{\gamma-1}{2} M_j^2\right]^{\frac{\gamma+1}{2(\gamma-1)}}, \quad (21)$$

illustrating that k and A_j+S_j depend on the two unknowns p_j and M_j . A close look at Eqs. 18 to 21 will reveal that the four unknowns p_j , M_j , k , and A_j+S_j can be manipulated into one equation for M_j and solved iteratively.

If the solution for M_j turns out to be subsonic, for which this analysis is valid, then p_j , ρ_j , a_j , u_j , A_j+S_j and k are readily determined from the past equations. On the other hand, if M_j is found to be supersonic, then simply set M_j to minus unity (which bypasses the head-loss equation) and again proceed to find p_j , ρ_j , a_j , u_j and A_j+S_j . This completes all of the jet flow conditions, and the combined jet area A_j+S_j is also determined.

If the inflow entrance on the RWE is well rounded so that jet inflows do not contract, then the combined eliminator area A_e+S_e is equal to A_j+S_j . On the other hand, if the inlet edges on the RWE are sharp, then a contraction coefficient has to be applied. For a Borda inlet flow¹⁴ this would be given by

$$C = \frac{1}{\gamma M_j^2} \left[\left(1 + \frac{\gamma-1}{2} M_j^2 \right)^{\gamma/(\gamma-1)} - 1 \right], \quad (22)$$

or in a more convenient and yet accurate expanded form as

$$C = \frac{1}{2} + \frac{M_j^2}{8} + \frac{(2-\gamma)M_j^4}{48} + \frac{(2-\gamma)(3-2\gamma)M_j^6}{384}. \quad (23)$$

Then the total RWE area A_e+S_e is equal to $(A_j+S_j)/C$.

In general the inlet edges are partly rounded, and C lies somewhere between the maximum value of unity for well-rounded inlets and the lower value given by equations 22 or 23. In such cases, the value from equations 22 or 23 can be modified by again using the expression $C + \omega(1-C)$, where the parameter ω is given empirically by $1 - \exp(-90R_o/D_h)$, where R_o is a typical value of the radius of rounding on the inlet edges and D_h is the hydraulic diameter of the combined vented areas.

In this inflow analysis no distinction has been made between A_j and S_j . They have simply been combined as a total inflow area. This is partly due to the flow coming from the atmosphere and partly because no theory is presently available or has been recently devised that would permit one to treat the end and side inflows separately.

3.2 UNSTEADY-FLOW ANALYSIS

The analysis for nonstationary flows inside shock tubes and blast wave simulators is needed to predict the transient wave motion from the interaction of shock or blast waves with the RWE having side and end vents. Unsteady wave motion will produce transient waves with amplitudes and signatures that cannot be predicted by the quasi-steady analysis of the last section. The unsteady flows in shock and blast tubes are solved spatially and temporally by using the random-choice method (RCM), which is based on the explicit solution of Riemann problems for each cell and quasi-random sampling. Riemann problems are solved with area changes included directly, whereas other source terms from friction, heat transfer, mass addition, and head losses are included with the old scheme of operator splitting in time. Although the RCM has been improved especially for this study, the best reference is still the report by Zhang and Gottlieb.¹⁵

3.3 EXAMPLE RESULTS OF QUASI-STEADY AND UNSTEADY ANALYSES

The first example illustrates the importance of including contraction coefficients with the free jets. The simple case of a flat-topped shock wave incident on an RWE with an end vent only is considered, and the vent area is determined such that there is no reflected wave (except for a short transient spike). The results for the area ratio A_e/A_c versus incident shock strengths p_2/p_1 are shown in Figure 4. The case of perfectly sharp vent edges corresponds to $\omega = 0$ and well rounded edges are given by $\omega = 1$. The spread in these curves shows the effects of different degrees of vent edge rounding, and the effects are by no means negligible. Hence, they should be included in RWE analyses to obtain realistic results. For example, for a shock

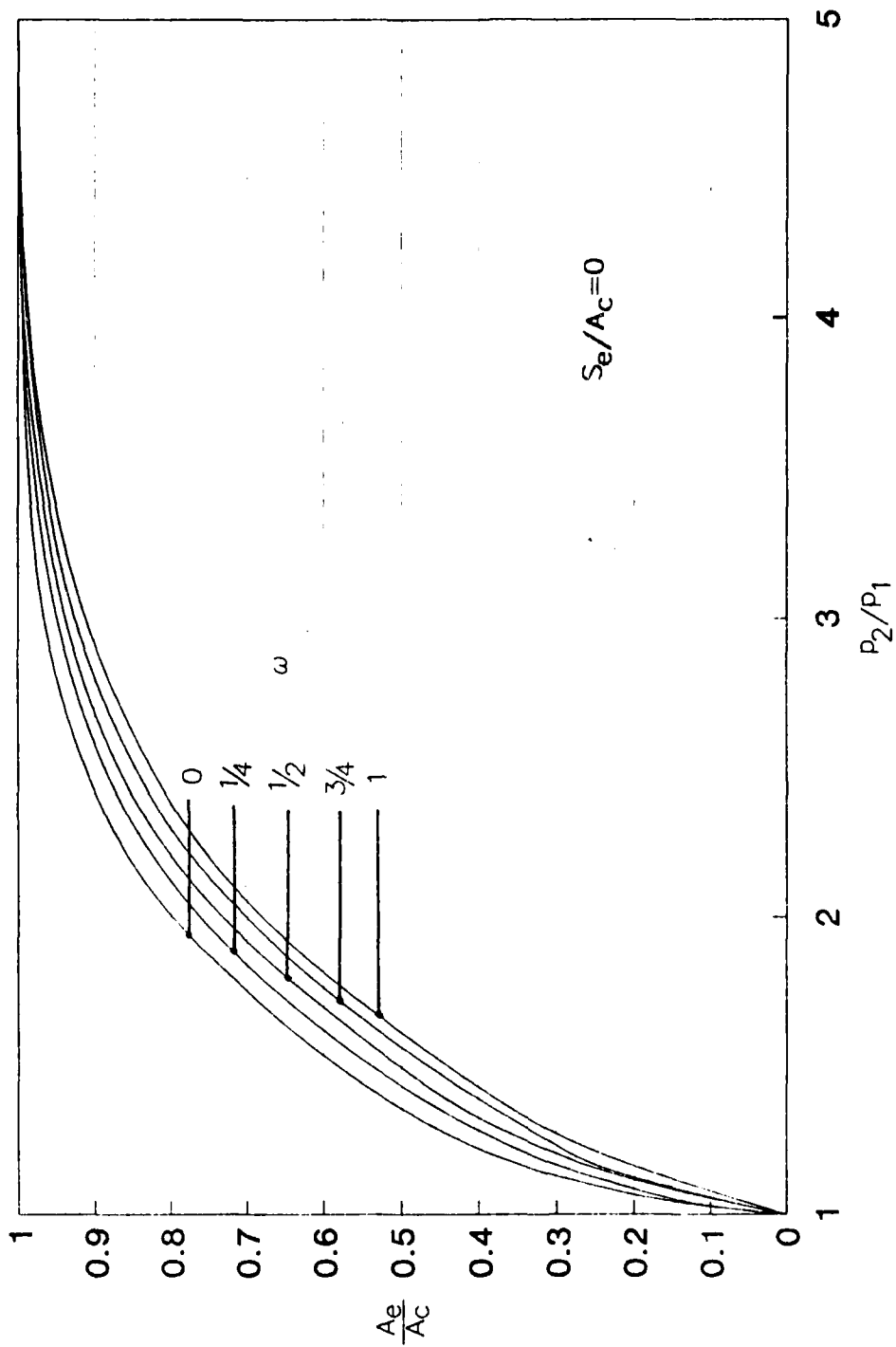


Figure 4. Area setting for a reflection eliminator with an end vent only which produces no reflected wave (except for the spike).

strength p_2/p_1 of 2, the area ratio A_e/A_0 varies from 0.72 to 0.84 (by about 16%).

It is interesting to see that the area ratio A_e/A_0 is very small for weak shock waves and increases toward unity as p_2/p_1 goes to 4.8232. At this shock pressure ratio the flow behind the shock just becomes sonic, and at higher values the flow is supersonic. The RWE is not required for sonic and supersonic outflows because the reflected rarefaction wave travels at the local sound speed and cannot move upstream. (In fact, it is swept downstream to become an oblique expansion wave.)

RWEs normally have vent edges with a fixed radius of rounding, rather than a constant value of ω . Hence, the area ratio A_e/A_0 for a particular shock tube and RWE with an end vent only is shown in Figure 4. These dashed line results are for a shock tube that is 64 mm high and 38 mm wide, and the vent takes the form of a long vertical slot having a small rounding radius of 0.4 mm. In the case of weak shocks ($p_2/p_1 = 1$) the RWE area is almost zero and even a small radius of rounding appears to be very large or well rounded as compared to the small width of the slot. Hence, the dashed line follows the line for $\omega = 1$ for well rounded vent edges at the bottom of the figure. For stronger shocks the vent slot becomes larger and the radius of rounding appears smaller in comparison to the slot width. Hence, the dashed line cuts across the various lines for ω and eventually comes close to the line for $\omega = 0$ (as shown in Figure 4).

It is interesting to illustrate how sensitive the reflected wave amplitude is to a mis-setting of the RWE area. To achieve this, let the reflected wave have specified strengths given by $p_3 - p_2 = \eta(p_2 - p_1)$, where η equals 0, ± 0.05 and ± 0.10 . Hence, the jump in pressure across the reflected wave is a percentage of that across the incident shock. The upper dashed and dotted lines correspond to the case of reflected rarefaction waves, since the vent area was too large, whereas the bottom dashed and dotted lines are for the case of reflected shocks, because the vent area was too small. These results show the sensitivity of the

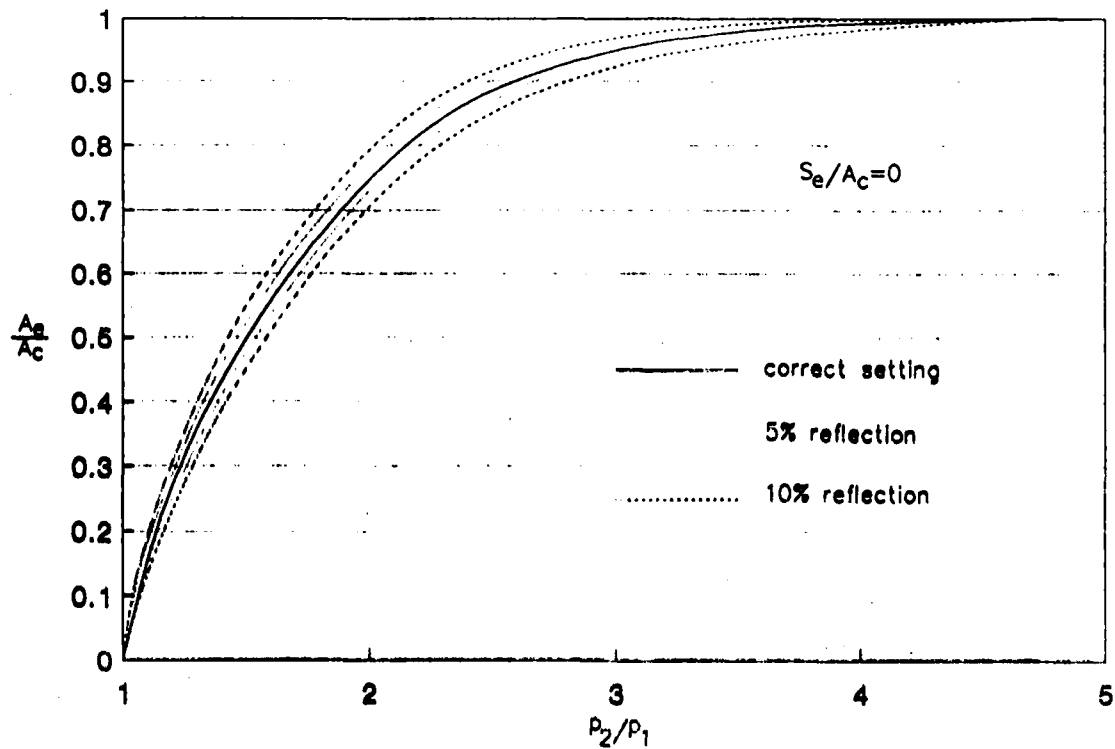


Figure 5. Sensitivity of reflection eliminator area setting (end vent) in producing a reflected wave.

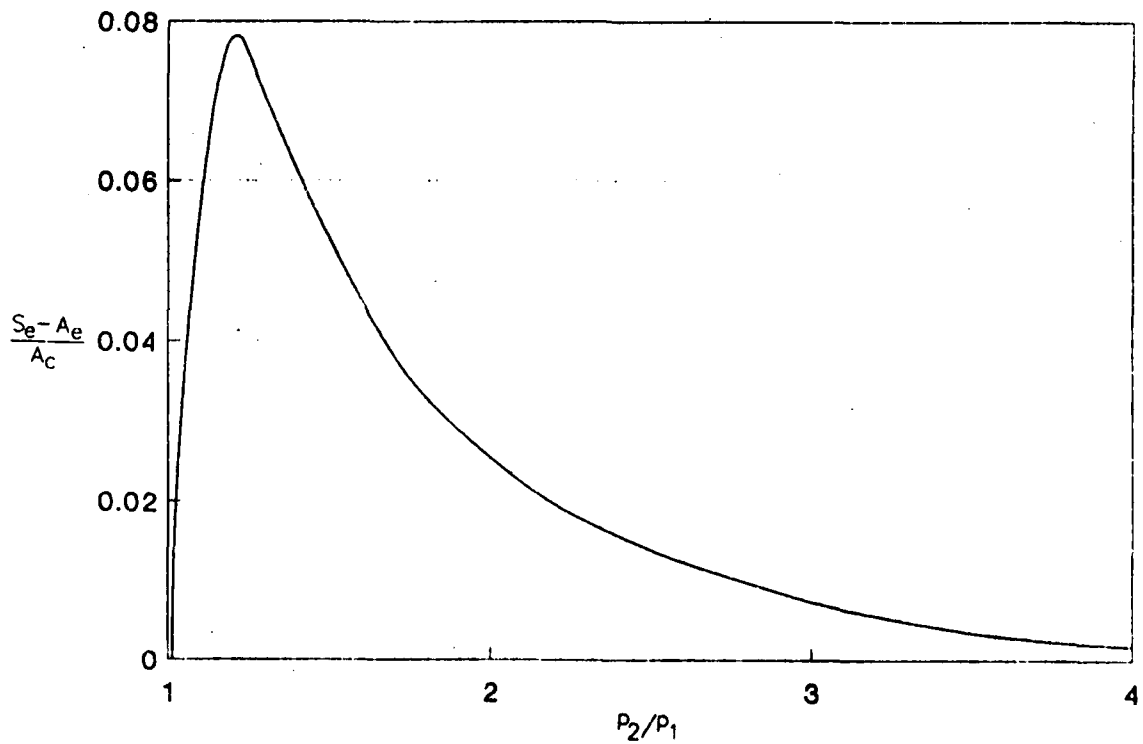


Figure 6. Difference in vent areas from using either an end vent (A_e) or side vent (S_e) in the reflection eliminator.

strength of the reflected wave to any mis-setting of the vent area. A close look at these results will show that a 5% mis-setting in area will produce a reflected wave overpressure about 5% of that of the incident shock. Hence, the amplitude of the reflected disturbance is fairly sensitive to any mis-setting of the RWE vent area.

The results given in Figures 4 and 5 for an RWE with an end vent only have been repeated for the case of a side vent only. However, the differences are rather small and are not presented. For all incident shock strengths the side vent needs a slightly larger area, mainly because the free jet is inclined rather than being perpendicular to the tube axis, which acts like an additional contraction effect since $S_e = S_j / [C_s \sin(\alpha_j)]$. This extra area is illustrated best by plotting $(S_e - A_e) / A_c$ versus p_2/p_1 , where S_e and A_e are the side and end vent areas if each is used alone to produce no reflected waves for the previous shock tube (64 mm high and 38 mm wide). These results are shown in Figure 6. The additional area for the side vent over the end vent is a maximum of about 8% at a shock strength of 1.2, and less than this for lower and higher values. If the shock tube were square or round instead of rectangular, then the differences would be even smaller (with a maximum typically less than 4%).

From results such as these one can conclude that an RWE with either end or side vents will give virtually the same performance, and so will a combination of end and side vents. Whether more or less area is shifted from the end vent to the side vent will not affect the performance. However, there may be advantages of putting more area in a side vent in the design of large RWEs.

Now consider the case of a simulated blast wave with a decaying profile, and some results for an active RWE. Let the flow properties be known entirely at a location 20 m beyond the test section, for the case when the duct extension is sufficiently long that no reflection has returned to affect these flow properties. Sample pressure and flow velocity signatures are presented in Figures 7a and 7b. The peak overpressure of this wave is 1 atm, and the shock front arrival time t_a

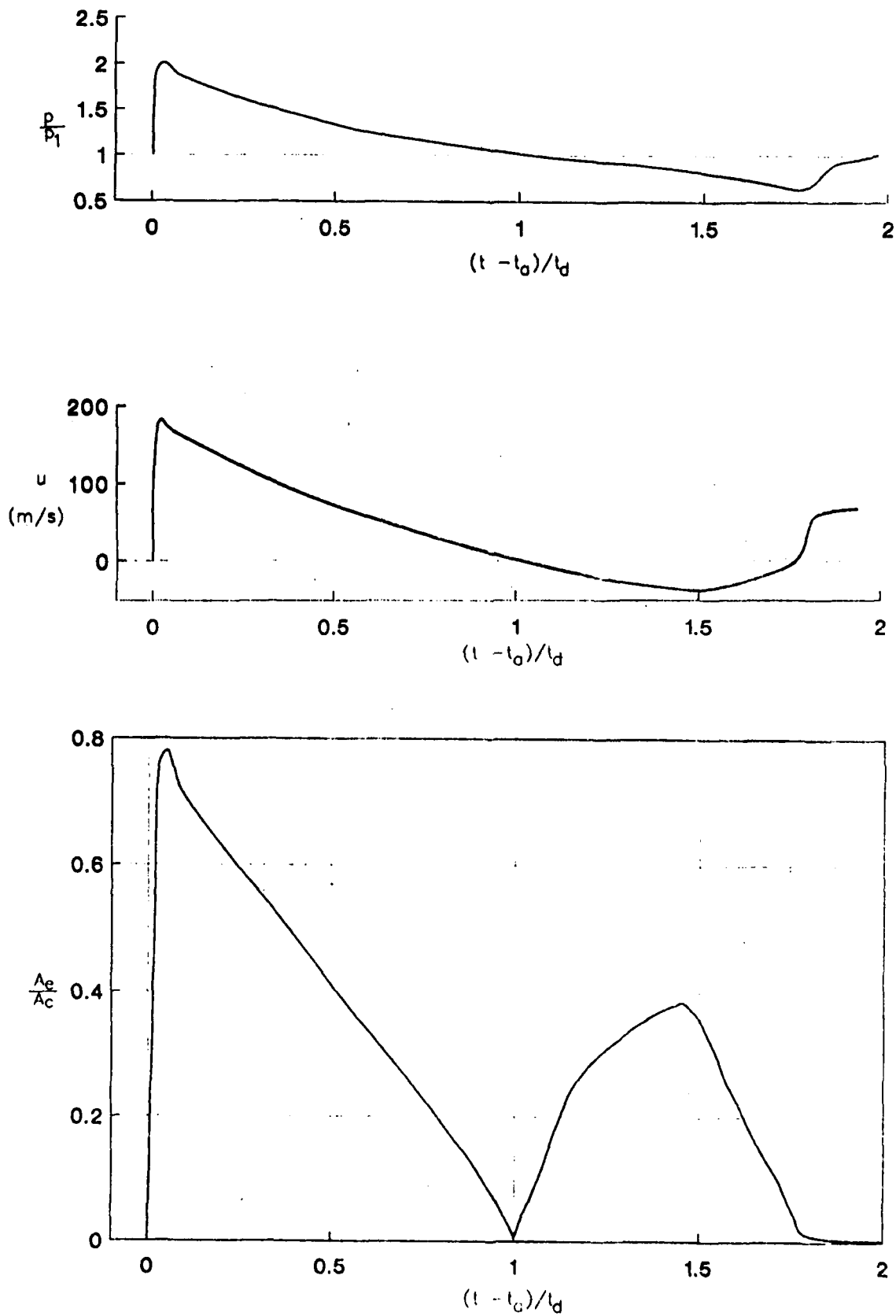


Figure 7. Area setting of an active RWE with sharp-edged end vents to eliminate reflections for the case of a decaying simulated blast wave.

and positive-phase duration t_d are fairly arbitrary. The duration could be 0.5 s for a low yield simulation, or 3 s for a high yield case. Note that for this weak blast wave case the durations of the overpressure, flow velocity and dynamic pressure signatures are all nearly equal.

Let the duct extension be terminated at the location where these results are known, and let an active RWE be installed (having sharp-edged end vents). If virtually perfect reflection elimination is to be achieved, then the RWE area setting with time must be that given in Figure 7c, according to the quasi-steady analysis. The vent area needs to be fairly wide open at 78% to handle the peak overpressure of the wave front, and then to decrease more or less linearly to zero as the outflow during the positive phase diminishes to zero. The vent area must then increase to a maximum of 38% open for the case of inflow during the first half of the negative phase of the velocity, and thereafter decrease back to zero when the flow velocity returns to zero. After this the overpressure and flow velocity have the opposite sign, and continued perfect reflection elimination is not possible. In this particular case the RWE is best kept closed. This RWE area setting with time is fairly typical for the case of simulated blast waves. Because of the large vent area variation that is needed to eliminate the reflection, it is fairly obvious that a passive RWE will not perform well and an active RWE is required.

The area setting was predicted with the quasi-steady analysis, and it is worth proving that this method of obtaining the RWE area setting with time is essentially correct for achieving a good reflection elimination. Hence, the unsteady analysis is used to determine the flow in a blast simulator, as the incident blast wave travels along the duct, interacts with an active RWE using the predicted area setting with time, and produces a reflected wave at the test section. These results are given in Figure 8, along with other interesting results for the cases of an open end and a passive reflection eliminator. The reference case for the pressure and flow velocity signatures is the infinite duct extension (solid line), because no reflection is present at the test section. In

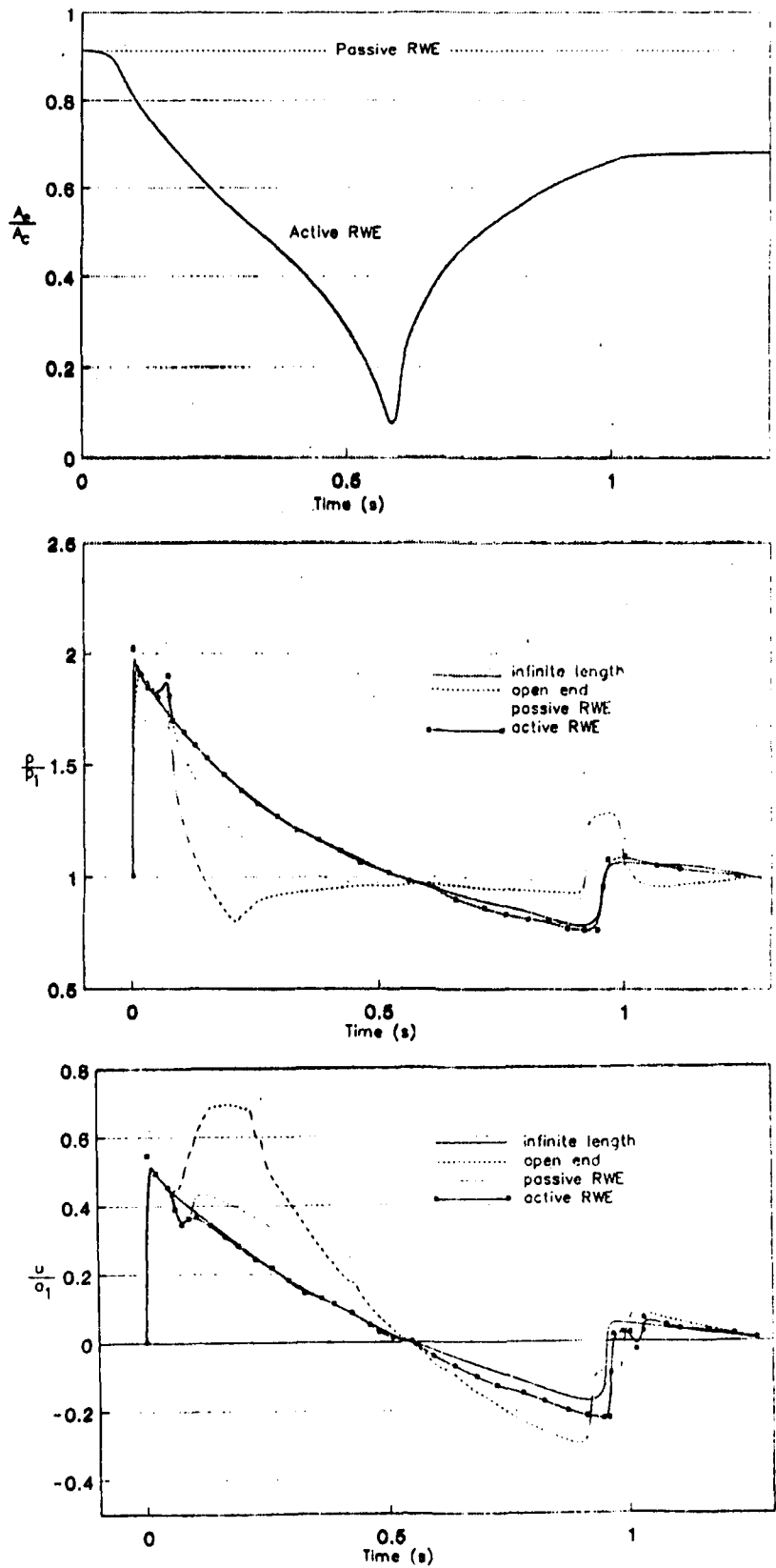


Figure 8. Pressure and flow velocity signatures for the cases of an infinite duct extension, open end, passive RWE, and active RWE

the case of an open end there is a severe drop in pressure and rise in flow velocity on arrival of the reflected wave, and the need for an RWE is obvious. A passive RWE set at a vent area to accommodate the peak overpressure of the blast wave is helpful in weakening the reflection, but the reflection is still significant because a much smaller vent area is needed at later times. An active RWE is excellent in eliminating the reflection. In the positive phase there is only an overshoot or a spike near the front of the wave, caused by the transient interaction of the incident shock front with the area reduction of the RWE. In the negative phase for the case of inflow, there is a minor reflection most noticeable in the flow velocity signature. This slight lowering of the signature is mostly due to not reducing the vent area exactly to zero at a time of about 0.6 s.

The main conclusion concerning the quasi-steady and unsteady analyses is that the former will predict the desired area setting for an active RWE to minimize the reflection, whereas the latter will predict the actual transient wave motion in the shock tube or blast simulator and provide an assessment of the capability of the RWE.

4.0 DESIGN CRITERIA

The RWE design concepts are tailored to fit the given data of the LB/TS: blast wave extreme conditions of overpressure and yield, and design of the LB/TS structure at the exit plane.

Safety, cost and rapid response of the RWE system to changing blast wave conditions are a major concern. There should be found, through a trade-off process, an optimum design for each concept, where each of these factors is addressed. A margin-of-safety factor of about 1.5 has been applied to all design calculations. Structural materials with yield strengths in the mid range for commercial steels have been specified to save cost and/or weight (see Table 1, as an example).

Fast installation and removal of the RWE is facilitated by mounting the structure on a wheeled carriage, use of quick attachments to the LB/TS structure and relatively low weight.

A goal of the design process was to counterbalance loads on the RWE wherever possible to reduce the power requirements of the RWE actuator system, as well as to save cost and weight for the entire structure.

5.0 ACTIVE RWE DESIGN ALTERNATIVES

Several design concepts for an active RWE were conceived and analyzed in the first phase of the contract. The first three concepts were designed for installation at the open end of the LB/TS and are therefore complementary to the use of the fourth concept: active or passive vents in the shell near the open end of the LB/TS. A description of the concept and a discussion of completed engineering analyses is presented for each of the three end-mounted designs.

5.1 ROTATING LOUVERS

The rotating louvers concept is a modification to the design used for the RWE on the French large diameter blast simulator at Centre d'Etude de Gramats (CEG)¹⁶ and consists of 100 horizontal louvers in eight columns, supported by nine vertical beams, each attached to prestressed cables passing through the LB/TS reinforced concrete shell¹⁷ (Fig. 9). The main differences between this RWE and the CEG device are that it covers a tunnel that is 2.4 times larger in area at 164 m², has fewer louvers (100 vs. 124), and uses diamond shaped louvers rather than flat plates. Seven of the nine vertical beams have a W shape (I-beam cross-section), while the two outermost beams have a WT shape (T-section). All the beams have a sloping front cover facing the flow as seen in Figures 10-13. The covers prevent stagnation pressure conditions from occurring across the entire face of the beam.

Each louver consists of a central hollow bar and four welded plates, forming a diamond cross-section (Fig. 14). The bar is mounted at both ends on bearings, located on the web of the beam (Fig. 10). At the end of each bar a gear is mounted, through which external torque is applied to rotate the louver.

Gear trains to operate adjacent sections of louvers are mounted on alternate beams (Fig. 10). In order to eliminate vertical forces acting on the louvers, vertically adjacent louvers (in the same column)

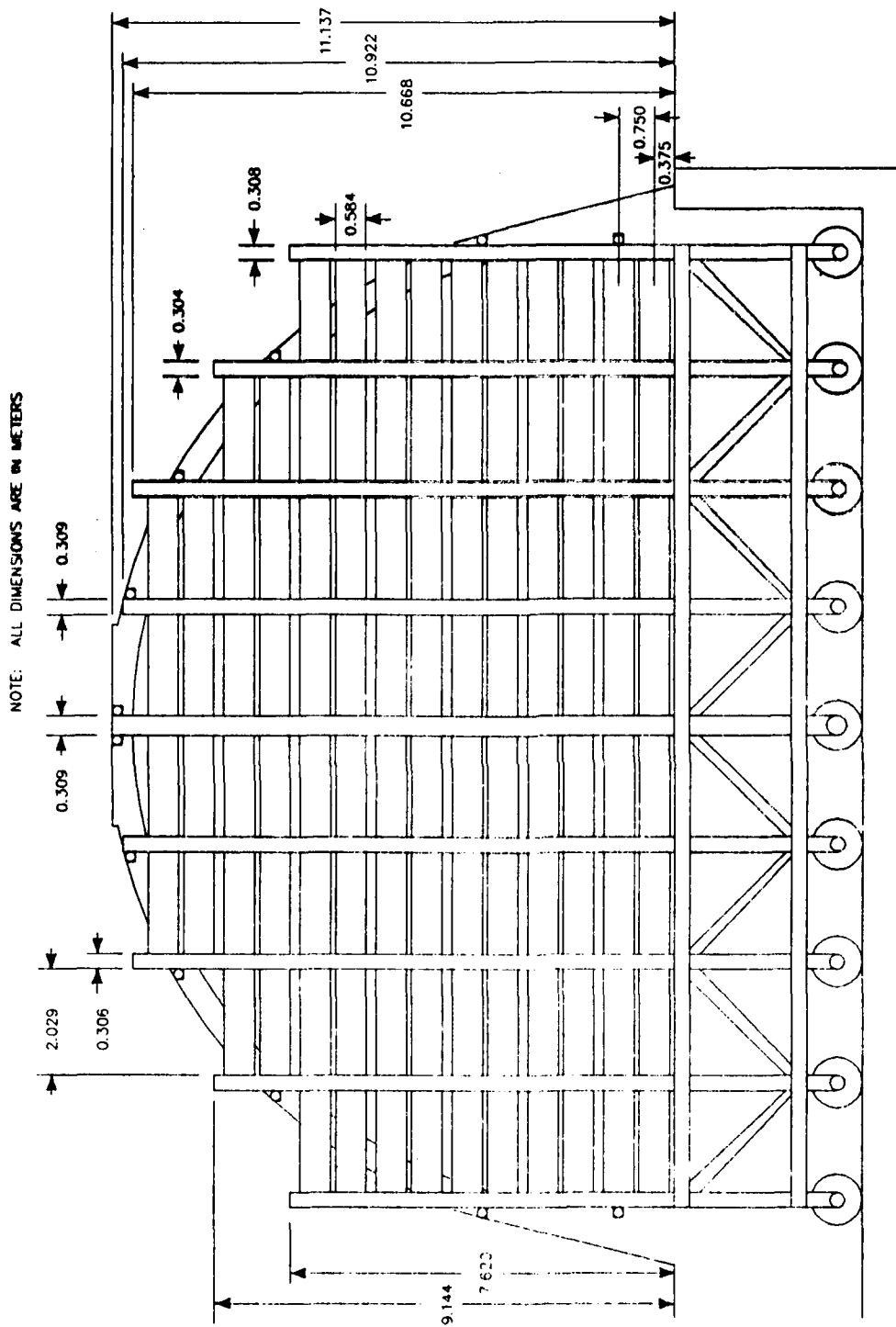
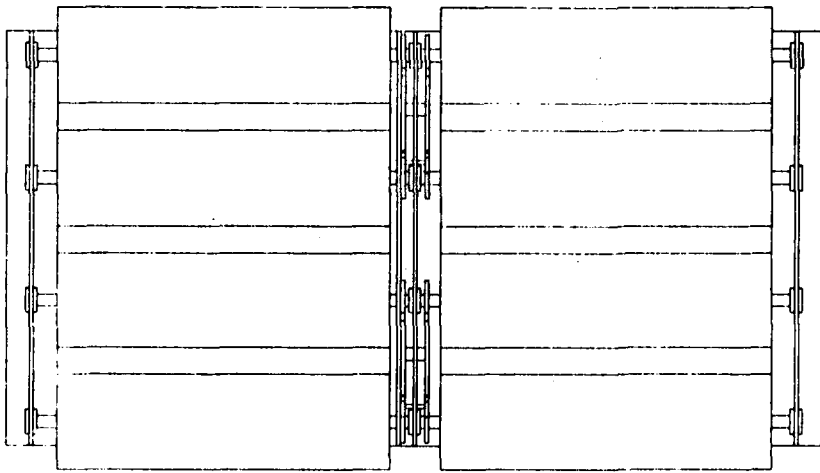


FIGURE 9: LB/TS ROTATING LOUVER REFLECTED WAVE ELIMINATOR EXIT PLANE

SECTION A-A



NOTE: FLOW DIRECTION →

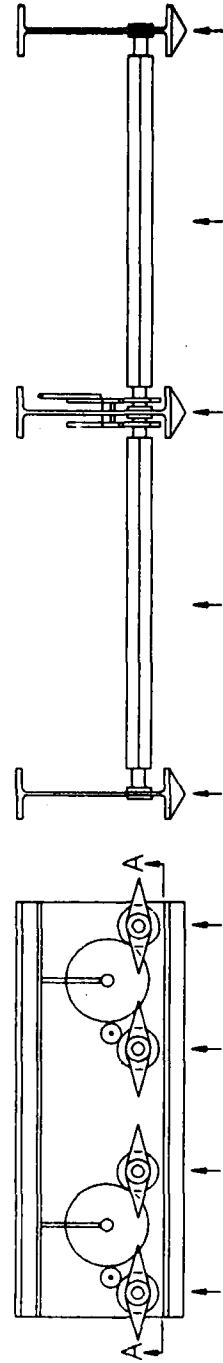


FIGURE 10: 3 VIEWS OF ROTATING LOUVER'S CONCEPT DESIGN

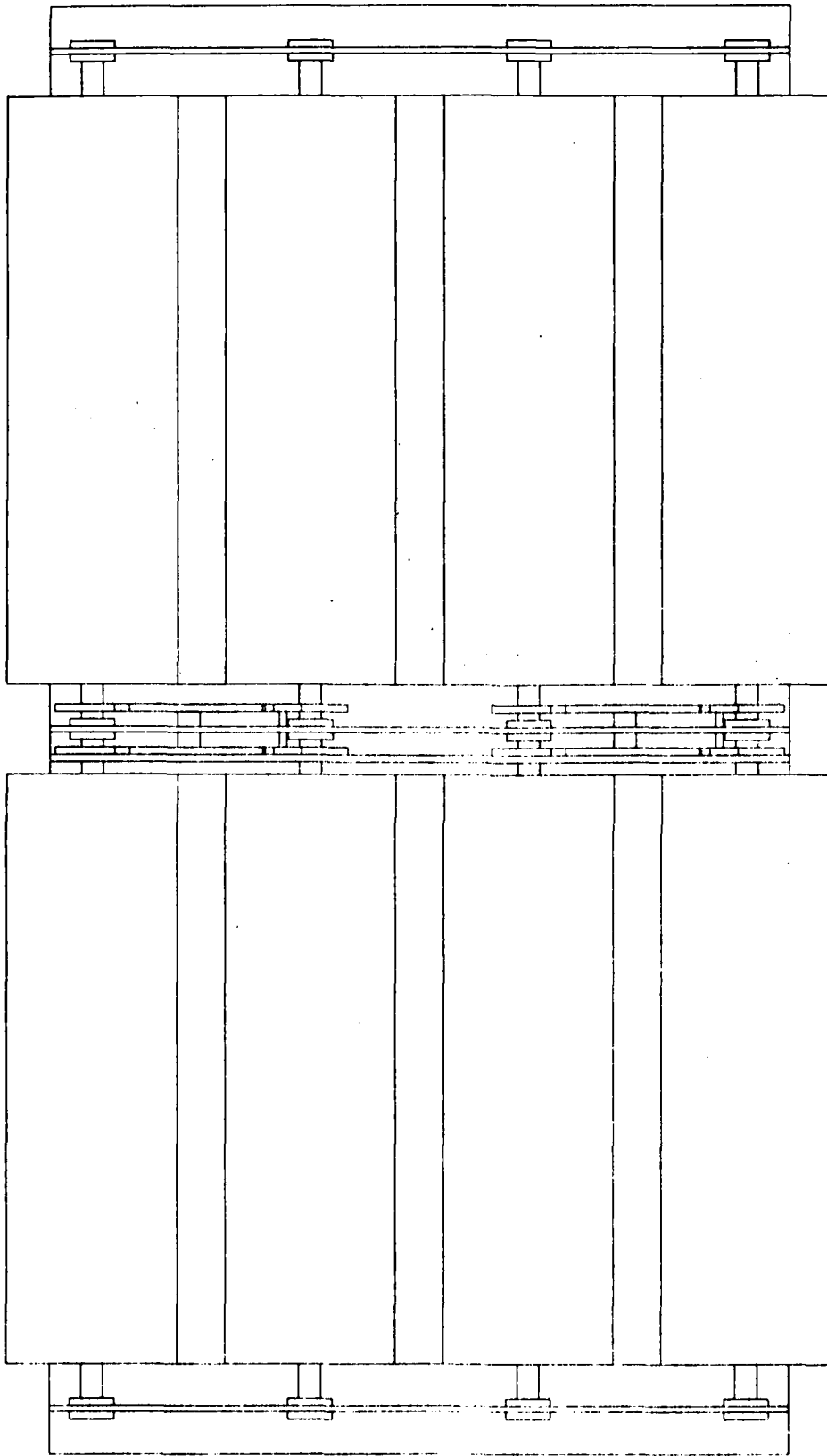


FIGURE 11: FRONT VIEW OF ROTATING LOUVER'S CONCEPT DESIGN

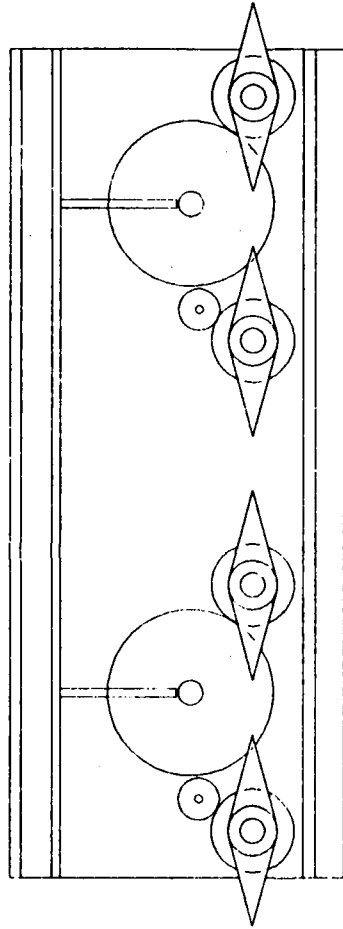


FIGURE 12: SIDE VIEW OF ROTATING LOUVER'S CONCEPT DESIGN

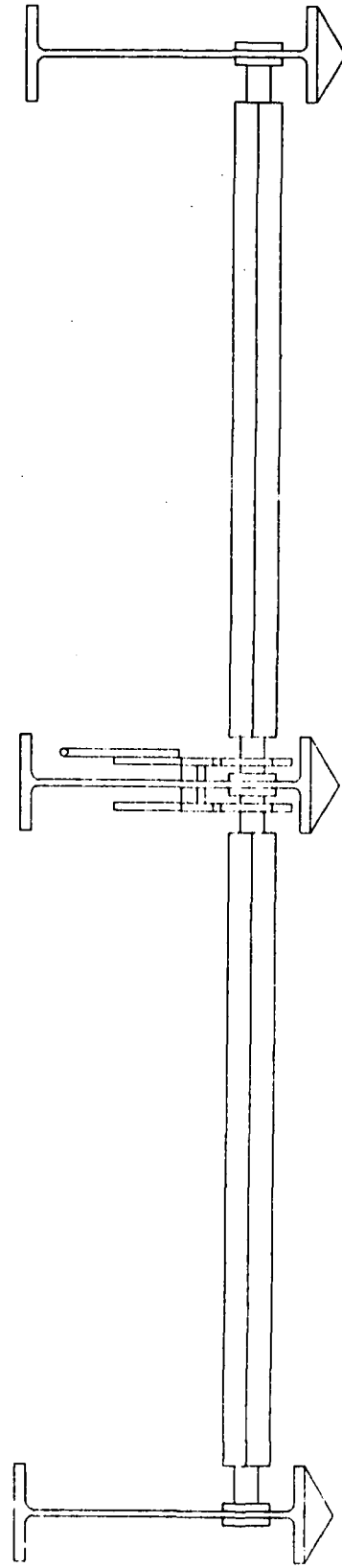
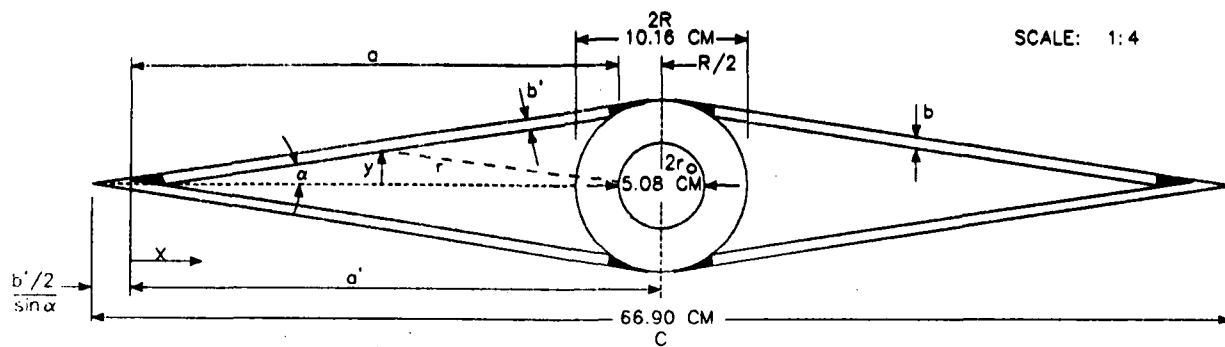
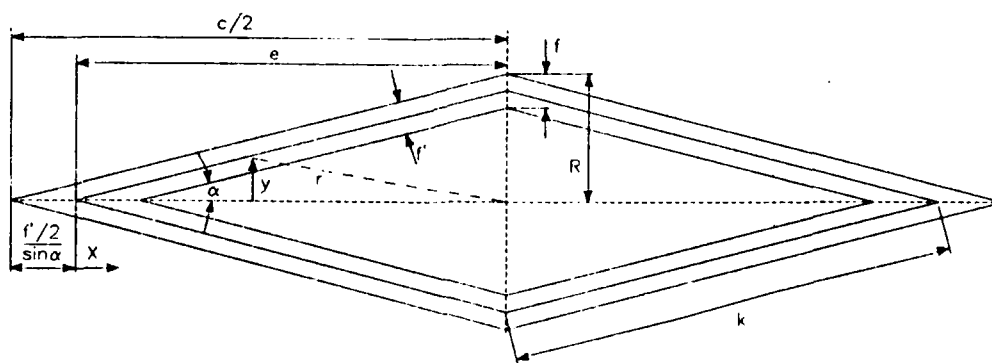


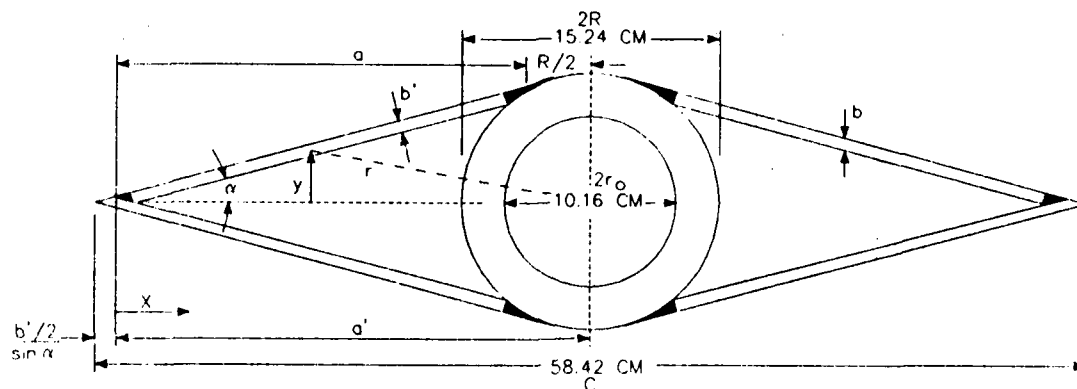
FIGURE 13: TOP VIEW OF ROTATING LOUVER'S CONCEPT DESIGN



14.c OPTIONAL ROTATING LOUVER



14.b NON-BAR LOUVER



14.a LOUVER WITH CENTRAL HOLLOW BAR

FIGURE 14: LB/TS REFLECTED WAVE ELIMINATOR COMPARATIVE ROTATING LOUVER'S CROSS SECTIONS

are driven in opposite directions by means of an additional small gear (Fig. 12).

The driving gears are operated by a hydraulically driven reciprocating rod through a lever attached to each pair of driving gears (Fig. 10). The reciprocating rods are actuated by a high pressure oil hydraulic system comprised of an accumulator, pump motor, and servo control valves operated under computer control.

The entire structure of the RWE and its required power system is mounted on a carriage (Fig. 9), to permit simple installation and removal of the active RWE system. Details of the carriage and power system were not designed under this effort.

The beams and louvers were structurally designed^{18,19} to withstand stresses exerted by the flow^{20,21,22} for the case of a 241 kPa/600 kT blast wave²³. The beams and louvers were assumed to be simply supported, situated in a full open condition at the time of arrival of the shock front. (Both the diffraction phase and drag phase of the loading were considered. However, this loading assumed the louvers were in a stationary position (zero degree angle of attack) through the duration of flow.) In a trade-off among stresses, weight and cost, commercially available high-strength, low-alloy steels²⁴ were selected for the louvers and for the support beams. The recommended members are noted in Table 1, as are the calculated loads and stresses. The total mass of the rotating louvers RWE system (carriage and hydraulic system excluded) is about 46721 kgs, of which 23587 kgs is the weight of the louvers, 20866 kgs the support structure and 2268 kgs the driving mechanism.

About 12.5% of the exit plane area is always closed, due to the vertical beams. The open area ratio (ratio of free area to total LB/TS cross-section) may vary between 69.2% when the louvers are fully open and 19.2% with louvers entirely closed (Fig. 10).

In order to size the components of the hydraulic system, the power required to rotate the louver elements of the RWE must be known. This can be calculated as the product of the torque and the angular

TABLE 1: SUPPORT BEAMS AND LOUVERS FOR THE LB/TS REFLECTED WAVE ELIMINATOR

Beam No.	Cross-Section Designation	Moment of Inertia (cm ⁴)	Effective Length (m)	Load-Force (KN)	ASTM Steel	Yield Stress, min. (mPa)	Max. Stress (mPa)	Margin of Safety
1 (Center)	W36x210	5.49x10 ⁵	10.75	2233	A572 Grade 60	414	280	1.47
2 and 3	W36x210	5.49x10 ⁵	10.50	2189	A572 Grade 60	414	268	1.53
4 and 5	W36x170	4.37x10 ⁵	9.50	1984	A572 Grade 60	414	272	1.51
6 and 7	W36x135	3.25x10 ⁵	7.75	1601	A572 Grade 50	345	237	1.45
8 and 9	WT18x97	3.75x10 ⁴	4.00	453	A572 Grade 50	345	227	1.51
Rotating Louver	(Fig. 14.a)	2963	2.029	252	A572 Grade 42	290	180	1.60
Optional Rotating Louver	(Fig. 14.c)	962	2.029	288	A514	655	424	1.54

velocity at any instant in time. For the double-symmetric diamond cross-section of the rotating louver, the blast wave aerodynamic forces are assumed to be applied through the center of rotation (which is optimistic since aerodynamic torques are assumed negligible). Therefore, the torque required to rotate the louvers (neglecting friction) is computed as the polar moment-of-inertia times the angular acceleration. Since the angular velocity and acceleration of the louvers vary as functions of the desired simulated blast wave overpressure, the required power is a time-varying quantity. The pressure/time profile for a 10kT, 241 kPa blast simulation was

calculated and used as input to the quasi-steady computer model prepared by UTIAS.²⁵ This model in turn calculated the open area ratio required for the RWE. Total duration of the positive phase for a 10 kT, 241 kPa blast wave is 289 milliseconds. Because of the relatively short duration, this simulation requires the most rapid changes in open area ratio, and therefore the greatest power requirement.

Given a louver cross-section, as shown in Figure 14, the polar moment-of-inertia of the entire RWE can be calculated for the 100 louvers. A computer program was written to calculate the power requirements as a function of time (and therefore of open area ratio) for rotation of a single louver. A sample output from the program for a blast wave simulating a 10 kT yield event at the 241 kPa overpressure level is presented in Table 2a. This output shows that the maximum power requirement for a 100-louver RWE design is 665 kw. However, this value does not account for losses in the gear train and associated linkage. It is important to note that the maximum power requirement is an artifact of the louver geometry. This is the case because of the specific angle-of-attack with the specified louver geometry. However, the large power requirement can be mitigated if another aspect of the RWE operation is considered.

The quasi-steady computer model allows the calculation of deviations in overpressure from the simulated profile when the RWE is not properly set to the required open area ratio. The deviations (penalties) for improper settings are significant when expressed as a percent of the overpressure profile, as high as -53% for an open area ratio of 10%, instead of the 3.9% required for proper RWE performance. However, this error is easily tolerated because the overpressure at this point in the simulated blast wave is a mere 413 Pa (0.06 psi), and the deviation, while large as a percentage of the overpressure, is insignificant in absolute value.

The net result is that the RWE can be designed to provide accurate open area ratios at high overpressures, and to close at slower rates

TABLE 2a. POWER REQUIREMENTS FOR ONE ROTATING LOUVER
FOR THE 241 kPa/10 kT CASE

Time (sec)	Required Theoret- ical Area Ratio	Achiev- able Area Ratio	Angle of Attack (deg) Theta	Angular Velocity (rad/sec) Omega	Angular Accelera- tion (rad/sec ²) Alpha	Required Power (Kw)
0.0000	.9888	.7393	15.13	0.00	0.00	0.000
.0150	.9677	.7393	15.13	0.00	0.00	0.000
.0300	.9342	.7393	15.13	0.00	0.00	0.000
.0450	.8887	.7393	15.13	0.00	0.00	0.000
.0600	.8831	.7393	15.13	0.00	0.00	0.000
.0750	.7696	.7393	15.13	0.00	0.00	0.000
.0900	.7065	.7065	17.84	3.16	210.36	2.535
.1050	.6561	.6561	22.09	4.95	119.45	2.257
.1200	.6078	.6078	26.29	4.88	-4.14	-0.077
.1350	.5610	.5610	30.51	4.91	1.55	.029
.1500	.5150	.5150	34.84	5.04	8.89	.171
.1650	.4698	.4698	39.33	5.23	12.39	.247
.1800	.4252	.4252	44.07	5.51	18.92	.398
.1950	.3810	.3810	49.17	5.94	28.43	.646
.2100	.3371	.3371	54.83	6.58	42.79	1.075
.2250	.2928	.2928	61.49	7.75	77.96	2.307
.2400	.2473	.2473	70.33	10.29	169.50	6.662

TABLE 2b. POWER REQUIREMENTS FOR ONE OPTIONAL ROTATING
LOUVER FOR THE 241 kPa/10kT CASE

Time (sec)	Required Theoret- ical Area Ratio	Achiev- able Area Ratio	Angle of Attack (deg) Theta	Angular Velocity (rad/sec) Omega	Angular Accelera- tion (rad/sec ²) Alpha	Required Power (Kw)
0.0000	.9888	.8022	8.74	0.00	0.00	0.000
.0150	.9677	.8022	8.74	0.00	0.00	0.000
.0300	.9342	.8022	8.74	0.00	0.00	0.000
.0450	.8887	.8022	8.74	0.00	0.00	0.000
.0600	.8831	.8022	8.74	0.00	0.00	0.000
.0750	.7696	.7696	11.03	2.67	177.70	2.082
.0900	.7065	.7065	15.51	5.22	170.51	3.914
.1050	.6561	.6561	19.17	4.25	-64.64	-1.208
.1200	.6078	.6078	22.75	4.17	-5.79	-.106
.1350	.5610	.5610	26.31	4.14	-1.50	-.027
.1500	.5150	.5150	29.92	4.20	3.82	.071
.1650	.4698	.4698	33.61	4.28	5.41	.102
.1800	.4252	.4252	37.40	4.41	8.71	.126
.1950	.3810	.3810	41.36	4.61	12.88	.261
.2100	.3371	.3371	45.54	4.87	17.68	.379
.2250	.2928	.2928	50.11	5.32	29.64	.693
.2400	.2473	.2473	55.31	6.05	49.02	1.304
.2550	.1987	.1987	61.76	7.50	96.84	3.194
.2700	.1429	.1429	71.52	11.35	256.34	12.787
.2850	.1050	.1050	83.83	14.33	198.74	12.518

than required near the end of the blast wave. The effect is to reduce the performance of the RWE, with minimal impact on the simulation.

An optional rotating louver design was prepared in order to extend the range of open area ratio from 75.75% in a fully open condition to 10% in the entirely closed position. The dimensions are presented in Figure 14 and on Table 3; the modified design is lighter, thinner and features a longer chord than the original louver design. The loads and stresses on the optional design are greater and thus require a grade ASTM A514 quenched and tempered alloy with a minimum yield stress of 95 ksi¹⁴.

The optional louver design (Table 2b) has a lower power requirement at all similar times than the baseline louver (Table 2a). At very late times the optional louver requires a large amount of power since it has a larger moment-of-inertia. However, since this louver is wider and has to move through a smaller angle of attack to achieve the same blockage, the moment-of-inertia is more than compensated for.

For comparison purposes, an alternate louver design consisting of four welded plates in a diamond cross-section, without the central bar (Fig. 14b), was evaluated. It was found that when using the same cross-sectional external dimensions and the same moment-of-inertia for the range of open area ratios, the alternate louver would weigh 23% more and its polar moment-of-inertia would be 93% greater than the central bar louver. Specific results of this analysis are presented in Table 3.

TABLE 3: COMPARISON RESULTS BETWEEN CENTRAL BAR AND ALTERNATE PLATE LOUVER CROSS-SECTIONS

Results	Plate (mm) Thickness	Weight (Kg)	Δ (%)	Polar Moment-of-Inertia (Kg.m ²)	Required Power, max (Kw)	Δ (%)
100 Louvers						
Central Bar	6.35	23678	--	3.98	665	--
Alternate Plate	19.33	29121	23	7.65	1283	93
Optional Rotating	6.35	19323	-18.4	4.56	1279	92

An analysis of aerodynamic flutter²⁶ was conducted for the rotating louver concept. The unstable divergent type of motion, when caused by aerodynamic forces resulting from vibrations, is called aerodynamic flutter. Flutter is one form of self-induced vibration, i.e., a type of vibration which sets up forces in phase with the displacement, which cause the vibration to persist and under some conditions to become divergent. Structures subject to flow should be examined for existing tendency to flutter in the flow conditions. Results are presented in Table 4 and indicate that there is no tendency of the rotating louver to flutter, since the greatest possible flow velocity (335 m/sec) is much smaller than the calculated divergence and flutter velocities.

TABLE 4: ROTATING LOUVER AERODYNAMIC FLUTTER ANALYSIS RESULTS

Natural Flexure (Hz) Frequency	Natural Torsional (Hz) Frequency	Divergence Velocity (m/sec)	Flutter Velocity (m/sec)	Peak Flow Velocity (m/sec)
82	125	2,235	1,534	335

The possibility of reducing weight by using a light material such as aluminum was also considered. Due to high stresses, high-strength aluminum would be required, which reduces weight but raises cost. However, with high strength aluminum, welding becomes a problem, which raises a major concern in the fabrication of the rotating louvers.

NOTE: ALL DIMENSIONS ARE IN METERS

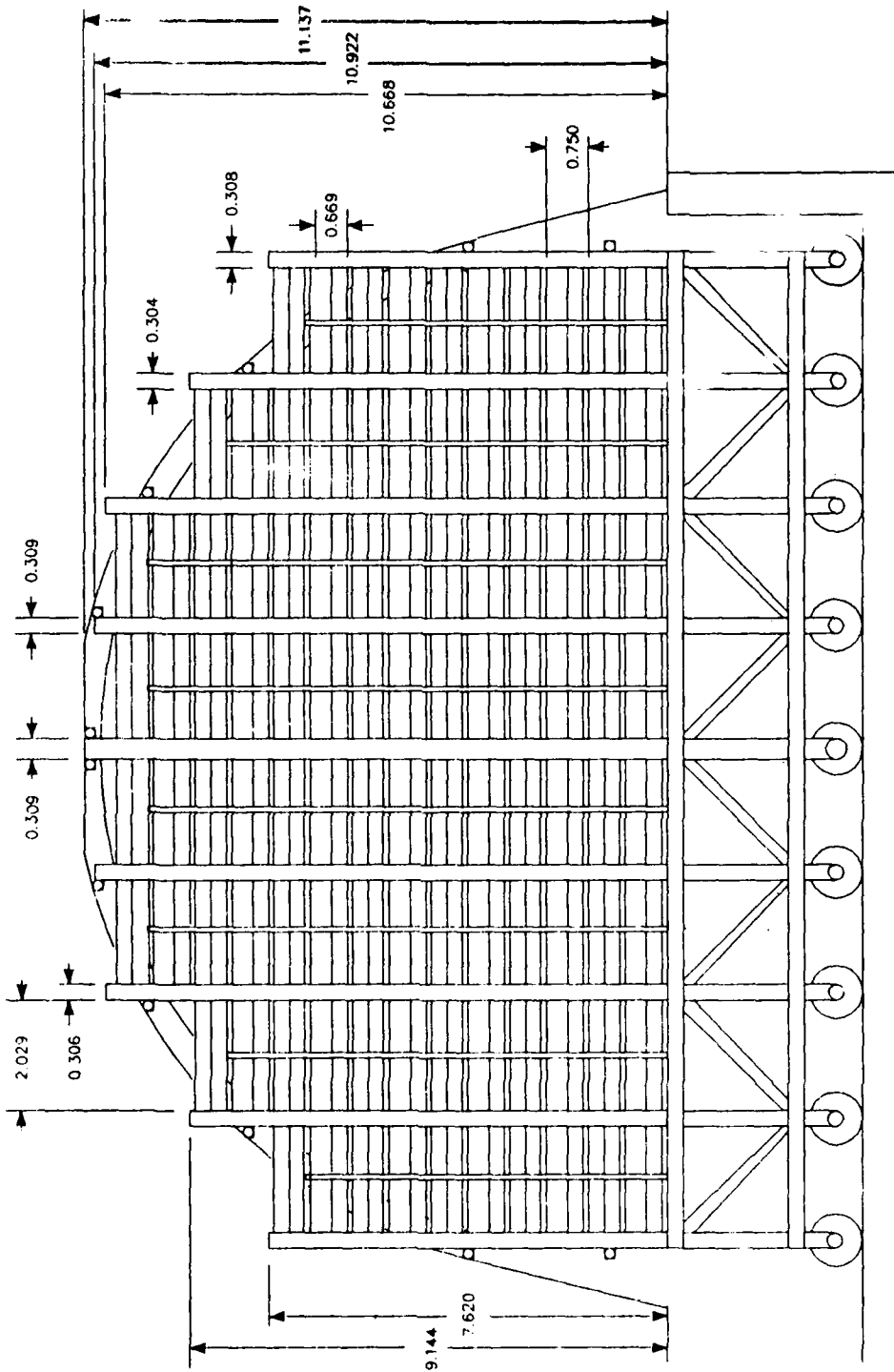
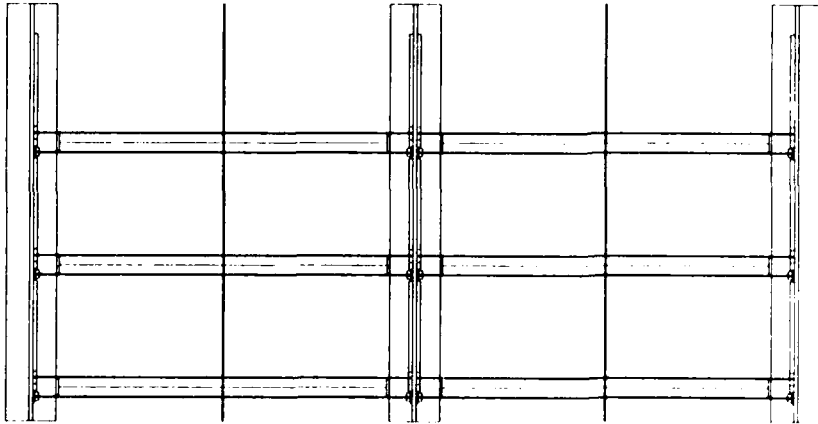


FIGURE 15. LB/TS HINGED LOUVER REFLECTED WAVE ELIMINATOR EXIT PLANE

SECTION A-A



NOTE: FLOW DIRECTION →

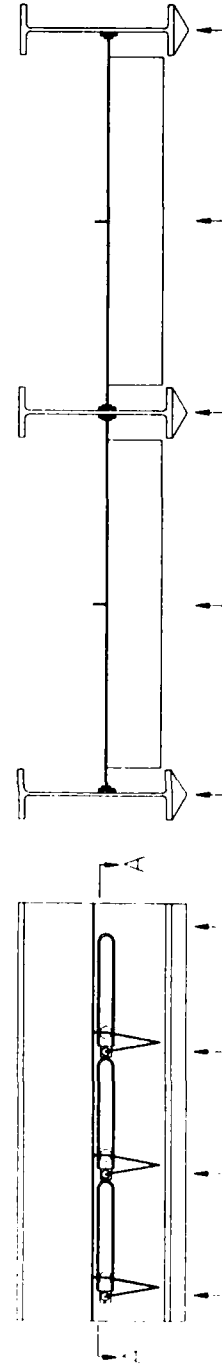


FIGURE 16. 5 VIEWS OF HINGED LOUVER'S CONCEPT DESIGN

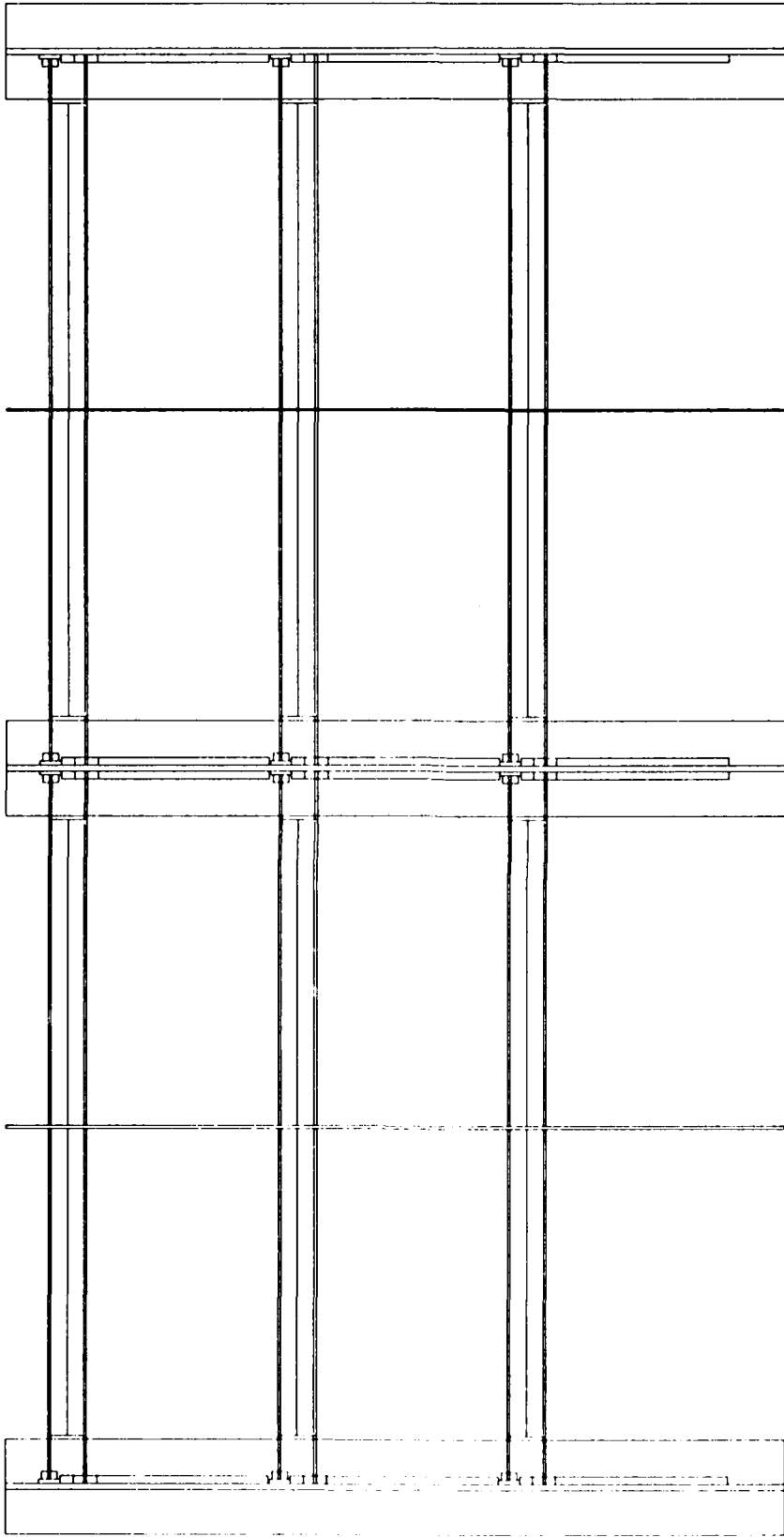


FIGURE 17: FRONT VIEW OF HINGED LOUVER'S CONCEPT DESIGN

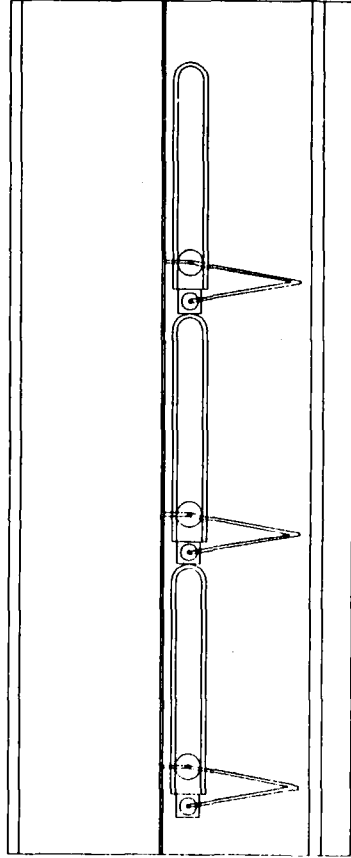


FIGURE 18: SIDE VIEW OF HINGED LOUVER'S CONCEPT DESIGN

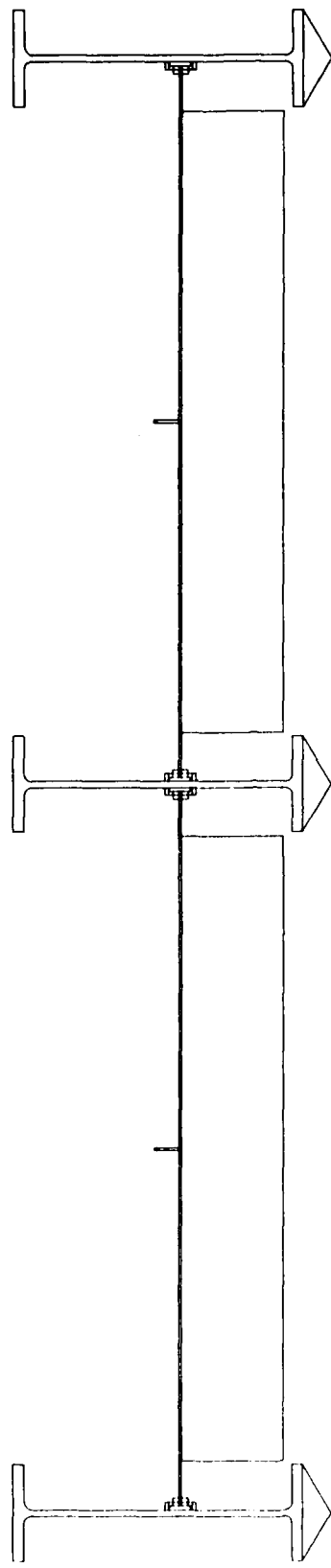
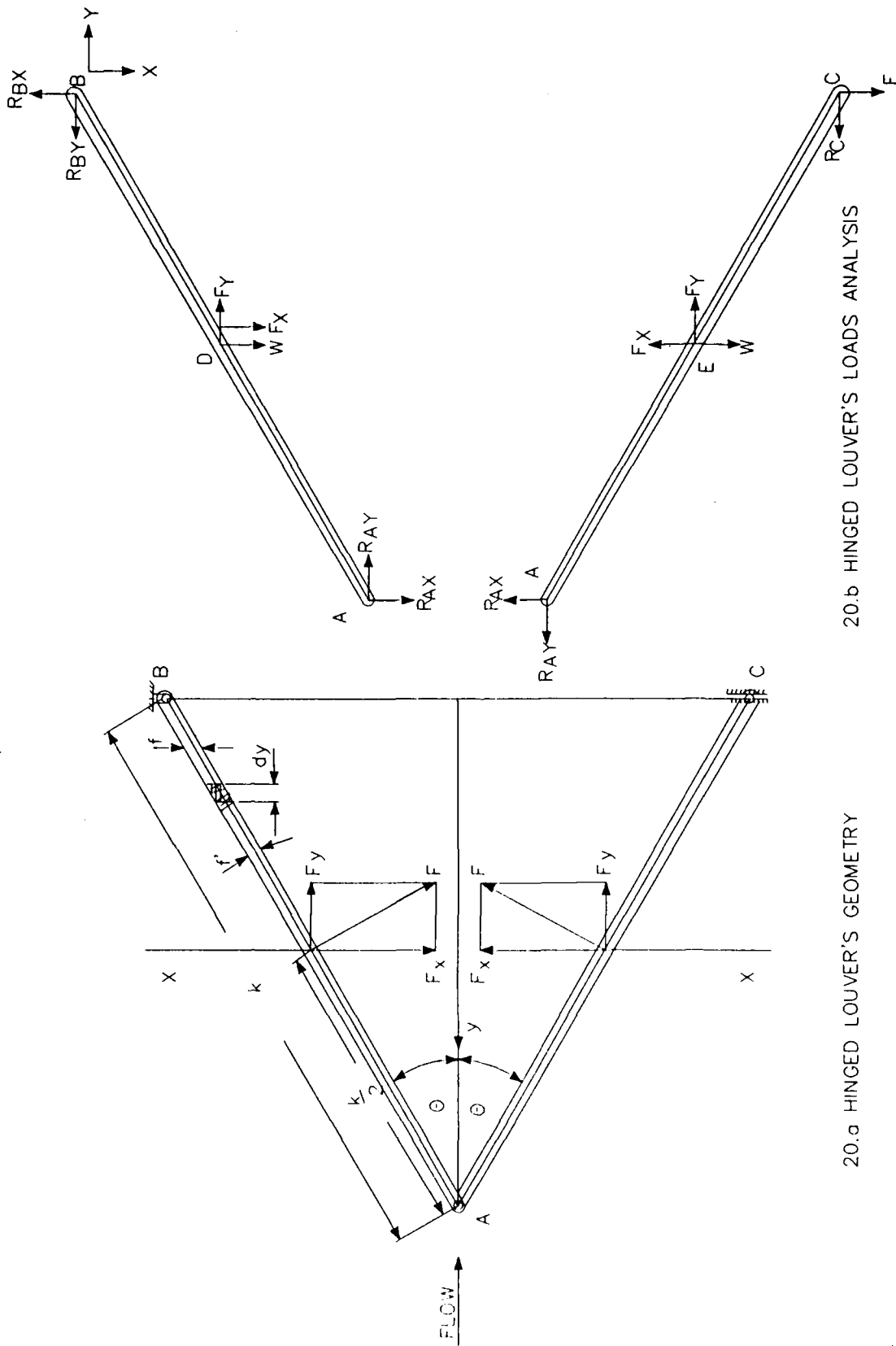


FIGURE 19: TOP VIEW OF HINGED LOUVER'S CONCEPT DESIGN



20.a HINGED LOUVER'S GEOMETRY

20.b HINGED LOUVER'S LOADS ANALYSIS

FIGURE 20: HINGED LOUVER'S GEOMETRY AND ANALYSIS

5.2 HINGED LOUVERS

The hinged louver concept is similar to the rotating louver, with the frontal area of the louver element changed by varying the angle between two plates hinged at one edge. The basic support structure of the hinged louver is shown in Figure 15. It is identical to that of the rotating louver RWE, which was described earlier. Figures 16-19 show the three views of the hinged louver concept design, whereas Figure 20 shows the basic shape of a single hinged louver in cross-sectional view. The open area ratio of the hinged louver will vary between 10% with louvers entirely closed and 85% when the louvers are fully open.

The hinged louver consists of two flat plates, which are pinned together at a hinge along the upstream edges. The upper plate is pinned to a vertical support beam, and the lower plate is attached to a control rod. The edge of the lower plate at the downstream side of the louver is limited to vertical motion only, moving in a smooth track, as detailed in Figures 18 and 19.

Each control rod operates one column of louvers (out of a total of eight) and is located at the midpoint of the section (Figs. 15 and 16), to minimize binding in the louver that could be generated if a controlling force was applied to either end of the louver.

In a trade-off among loads, weight and cost, the same steel as specified for the rotating louver was selected for the hinged louver. An analysis of the applied loads indicated that a minimum plate thickness of 8 mm is needed.

The total mass of the hinged louver RWE system (carriage and hydraulic system excluded) is about 30391 kg, of which 7711 kg is the weight of the louvers, 20865 kg for the beams, and 1814 kg for the driving mechanism.

An analysis of the loads applied to a single hinged louver was performed. The free-body diagram of Figure 20b was used to establish a

set of six equations that describe the forces and moments acting upon the two plates of the louver:

Upper Plate:

$$\Sigma F_X = R_{AX} + F_X + W - R_{BX} = \frac{W}{g} \ddot{X}_D \quad (24)$$

$$\Sigma F_Y = R_{AY} + F_Y - R_{BY} = \frac{W}{g} \ddot{Y}_D \quad (25)$$

$$\Sigma M_B = R_{AX} \cdot k \cos\theta + R_{AY} \cdot k \sin\theta + (F_X + W) \frac{k}{2} \cos\theta + F_Y \frac{k}{2} \sin\theta = I_{PB} \frac{d^2\theta}{dt^2} \quad (26)$$

Lower Plate:

$$\Sigma F_X = F + W - F_X - R_{AX} = \frac{W}{g} \ddot{X}_E \quad (27)$$

$$\Sigma F_Y = F_Y - R_C - R_{AY} = \frac{W}{g} \ddot{Y}_E \quad (28)$$

$$\Sigma M_A = F \cdot k \cos\theta + R_C k \sin\theta - (F_X - W) \frac{k}{2} \cos\theta - F_Y \cdot \frac{k}{2} \sin\theta = -I_{PA} \frac{d^2\theta}{dt^2} \quad (29)$$

A computer program was written to solve the six equations simultaneously. This program was coupled with a set of data that described the time dependence of the area ratio requirement for an active RWE to provide proper RW elimination for a 10 kT simulated blast wave. Aerodynamic forces were calculated based on both supersonic and slightly subsonic flow conditions. Separate coefficients of drag were established for each condition. For the supersonic condition the C_d was established with the louver at a zero degree angle of attack. In the subsonic condition the C_d was established assuming the louver was at a 15° angle of attack, where flow separation begins. Equations were included in the computer program that used this discrete data for blast wave time and corresponding area ratio to compute angular velocity and acceleration for the louver. It was then possible to calculate the power required for proper positioning of the hinged louver:

$$\text{Hydraulic Power} = F \cdot V = F \cdot X_{\dot{\theta}} = F \cdot 2k \cos\theta \frac{d\theta}{dt} \quad (30)$$

A second power requirement calculation was made based only on the polar moment-of-inertia of the hinged louver, which is a function of the half-angle between the two plates that form the louver (the angle θ in Fig. 20a). This alternate power calculation does not account for the pressure exerted on the hinged louver surface by the blast wave. This force is balanced in the rotating louver design because it is applied through the center of rotation, but that is not applicable in the hinged louver concept.

Results from the computer program are presented in Table 5. The power requirement is seen to be much larger than for the rotating louver, because the force resulting from the blast wave overpressure must be included. Comparison of the calculated power requirement with the alternate power (polar moment) calculation shows that most of the needed power is applied to oppose the moment generated by the blast wave overpressure. Especially noteworthy is the result that as the hinged louver nears full extension, the power must be applied in the opposite direction to reduce the rate at which the area ratio is changing. The large inertia power requirements near the end of the time period are due to the momentum of the previous motion of the hinged louvers and the help of the blast wave in closing the area. Due to this condition the requirement for additional hydraulic power to close the area is small. Design parameters for a 100-unit hinged louver RWE are presented in Table 6.

An analysis of aerodynamic flutter²⁶ was also conducted for the hinged louver concept assuming the following simplifications:

- a. natural flexure frequencies for a simple - supported beam, and
- b. natural torsional frequencies about the center-of-gravity axis.

The calculated divergence velocity for low values of the louver half angle is smaller than the flow velocity (Table 7). This result may indicate a potential for aerodynamic flutter at low louver angles that should be examined in further detail if the hinged louver concept is

TABLE 5. FORCE AND POWER REQUIREMENTS FOR ONE HINGED LOUVER (WITH RW JUMP) FOR THE 241 kPa/10 KT CASE

Time (sec)	Area Ratio	Angle of Attack (deg) Theta	Angular Velocity (rad/sec) Omega	Angular Acceleration (rad/sec ²) Alpha	Inertia Power (Kw)	Hydraulic Force (KN)	Hydraulic Power (Kw)
0.0000	.850	4.82	0.00	0.00	0.000	133.12	0.00
.0150	.850	4.82	0.00	0.00	0.000	92.43	0.00
.0300	.850	4.82	0.00	0.00	0.000	64.93	0.00
.0450	.850	4.82	0.00	0.00	0.000	45.62	0.00
.0600	.833	6.00	1.38	91.74	.432	34.02	30.90
.0750	.770	10.47	5.20	255.08	4.835	28.82	97.90
.0900	.707	14.98	5.25	2.85	.060	20.28	68.22
.1050	.656	18.65	4.27	-65.10	-1.204	14.87	39.93
.1200	.608	22.24	4.18	-5.97	-.118	11.62	29.85
.1350	.561	25.81	4.15	-1.67	-.036	8.46	20.98
.1500	.515	29.42	4.21	3.66	.088	5.86	14.26
.1650	.470	33.11	4.29	5.22	.141	3.72	8.87
.1800	.425	36.90	4.41	8.49	.259	2.01	4.71
.1950	.381	40.86	4.60	12.59	.439	0.65	1.51
.2100	.337	45.04	4.86	17.28	.697	-0.37	-.85
.2250	.293	49.59	5.30	29.02	1.396	-1.06	-2.42
.2400	.247	54.76	6.02	47.90	2.888	-1.44	-3.33
.2550	.199	61.15	7.43	94.15	7.654	-1.33	-3.18
.2700	.143	70.69	11.10	244.56	33.033	0.18	.45
.2850	.100	84.80	16.42	354.76	76.760	10.83	10.70

TABLE 6. ANALYSIS RESULTS FOR HINGED LOUVER GEOMETRY, WEIGHT AND MAXIMUM POWER REQUIREMENTS--FOR 100 LOUVERS

Plate (mm) Thickness	Plate (mm) Chord = k	Weight (Kg)	Polar Moment-of-Inertia, max. (Kg.m ²)	Inertia Power, max (Kw)	Hydraulic Power, max (Kw)
8	332	7802	13.7	7676	9790

selected for scaled tests. However, there are known techniques for flutter suppression that can be applied if a problem is confirmed.

TABLE 7. HINGED LOUVER AERODYNAMIC FLUTTER ANALYSIS RESULTS

Louver Half Angle (deg)	5	25	45	65	85
Natural Flexure Frequency (Hz)	189.4	172.3	134.4	80.3	16.6
Natural Torsional Frequency (Hz)	4.63	123.7	171.2	82.4	2.35
Divergence Velocity (m/sec)	<u>47.0</u>	1257.0	1754.0	838.0	23.9
Flutter Velocity (m/sec)	--	--	988.0	319.0	--
Flow Velocity (m/sec)	332-211	85.7	29.8	8.5	1.1

5.3 COMPARISON OF HINGED AND ROTATING LOUVERS CONCEPTS

Specific features of the hinged and rotating louver concepts are compared in Table 8.

TABLE 8: COMPARISON OF HINGED AND ROTATING LOUVERS

Feature Louver	RWE Mass (Kg)	Open-area Ratio Range (%)	Max. Power Req. (Kw)	Aero- dynamic Flutter	Louver Structure
Rotating	46720	20.5 - 74	665	No Tendency	Enclosed, Sturdy
Optional Rotating	42185	10 - 80	1279	No Tendency	Enclosed, Sturdy
Hinged	30391	10 - 85	9790	Some Tendency	Open on downstream side

The current design for the rotating louver RWE has no tendency for aerodynamic flutter and has a peak power requirement for the actuator system of less than 670 kw. The disadvantages of this design are a greater mass (46720 kg) and a smaller range of open-area ratios (20.5 - 74%). Modification to the rotating louver cross section extends the open-area ratio range to achieve 10 - 80% with a reduced weight louver. This bonus is obtained by reducing the central bar diameter and by extending the chord length, resulting in increased structural loads, which are matched by a better and more expensive steel alloy, as well as by a larger peak power requirement.

The current design of the hinged louver RWE has a lower mass (30391 kg) and a larger range of open-area ratios (10 - 85%) than the rotating louver concept. The disadvantages of this design are: a requirement for peak actuator power of over 9694 kw and an open louver structure, which causes a potential for aerodynamic flutter (at low louver angles). Some alternate hinged louver operator mechanisms were analyzed, resulting in the same conclusion. In order to move both hinged louver plates into the coming flow, there is a minimum power requirement which must be met and is actually the power requirement calculated earlier. However, design modifications may reduce or eliminate the hinged louver flutter potential.

5.4 STATOR-ROTOR CONCEPT

This RWE concept employs rotary motion of a radially segmented disc in the plane of the LB/TS exit to change the open area ratio.¹⁷ The stator, shown in Figure 21, is mounted to the LB/TS structure. The rotor, Figure 22, is mounted immediately downstream from the stator, and rotates on a central axis. Both assemblies consist of almost identical fan-shaped elements which partially block the open area of the shock tube exit. To change the open area ratio, the rotor is rotated relative to the stator to block additional area of the LB/TS exit plane. Figure

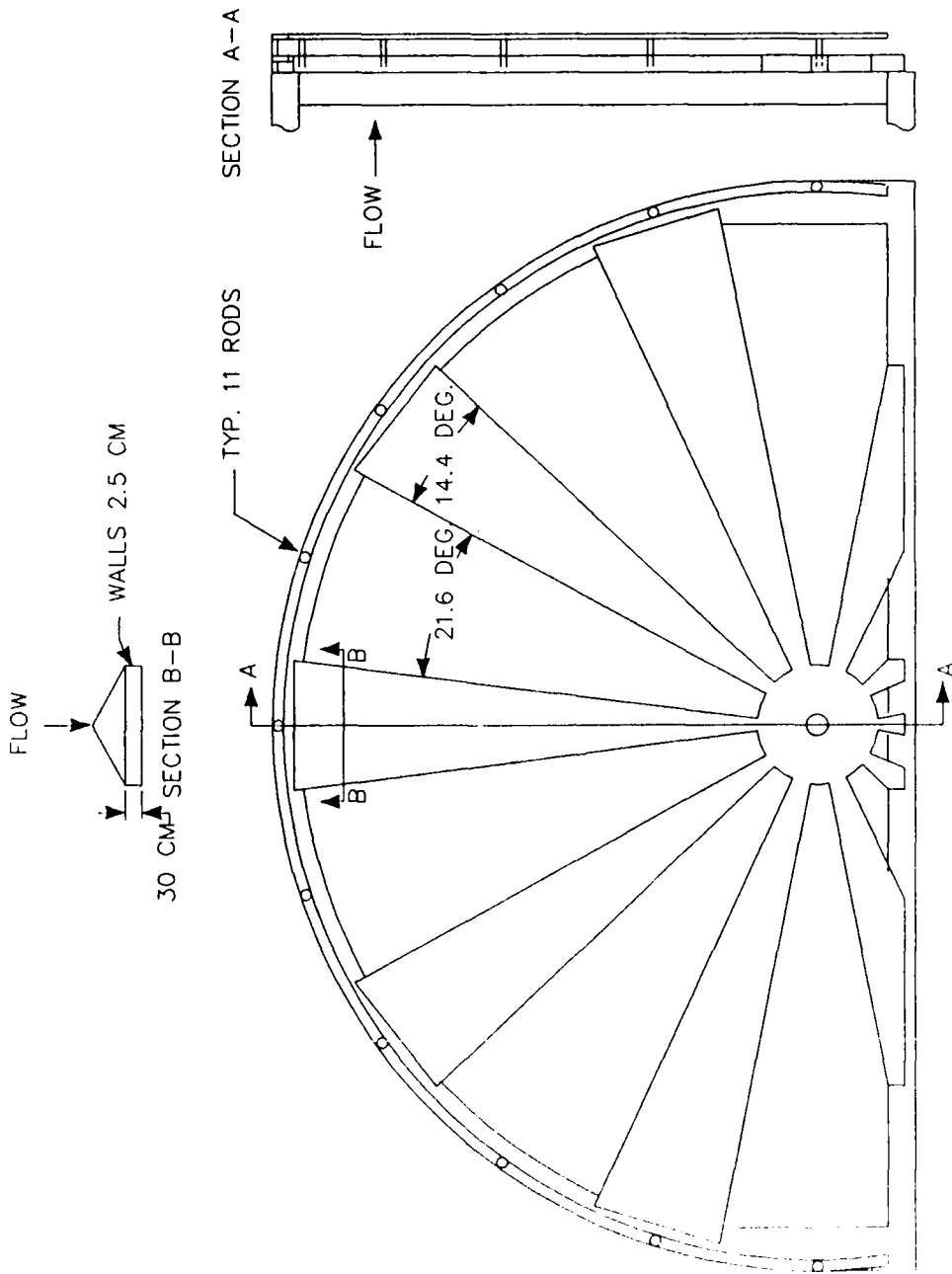


FIGURE 21: LB/TS REFLECTED WAVE ELIMINATOR STATOR DESIGN

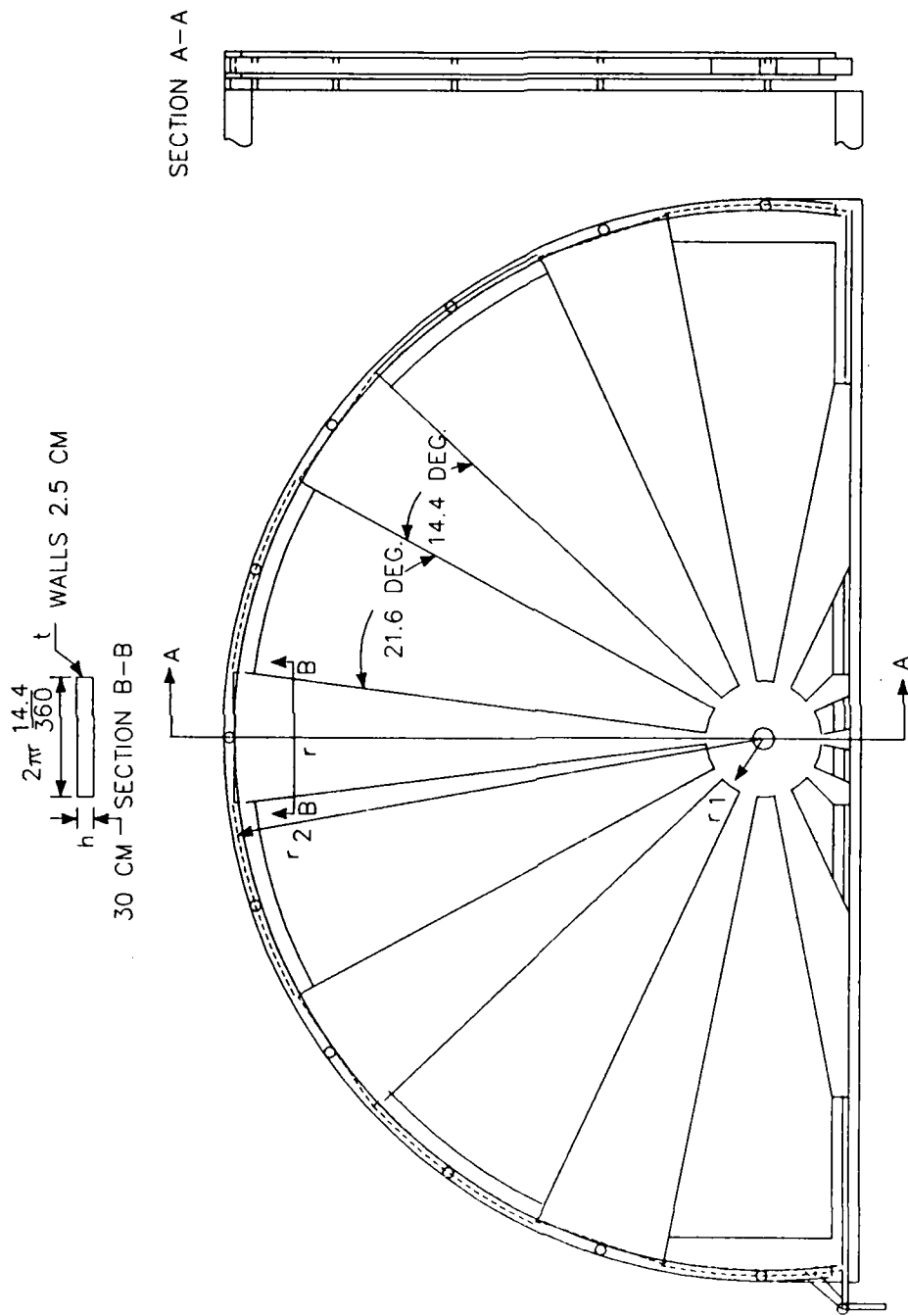


FIGURE 22: LB/TS REFLECTED WAVE ELIMINATOR ROTOR DESIGN

SECTION A-A

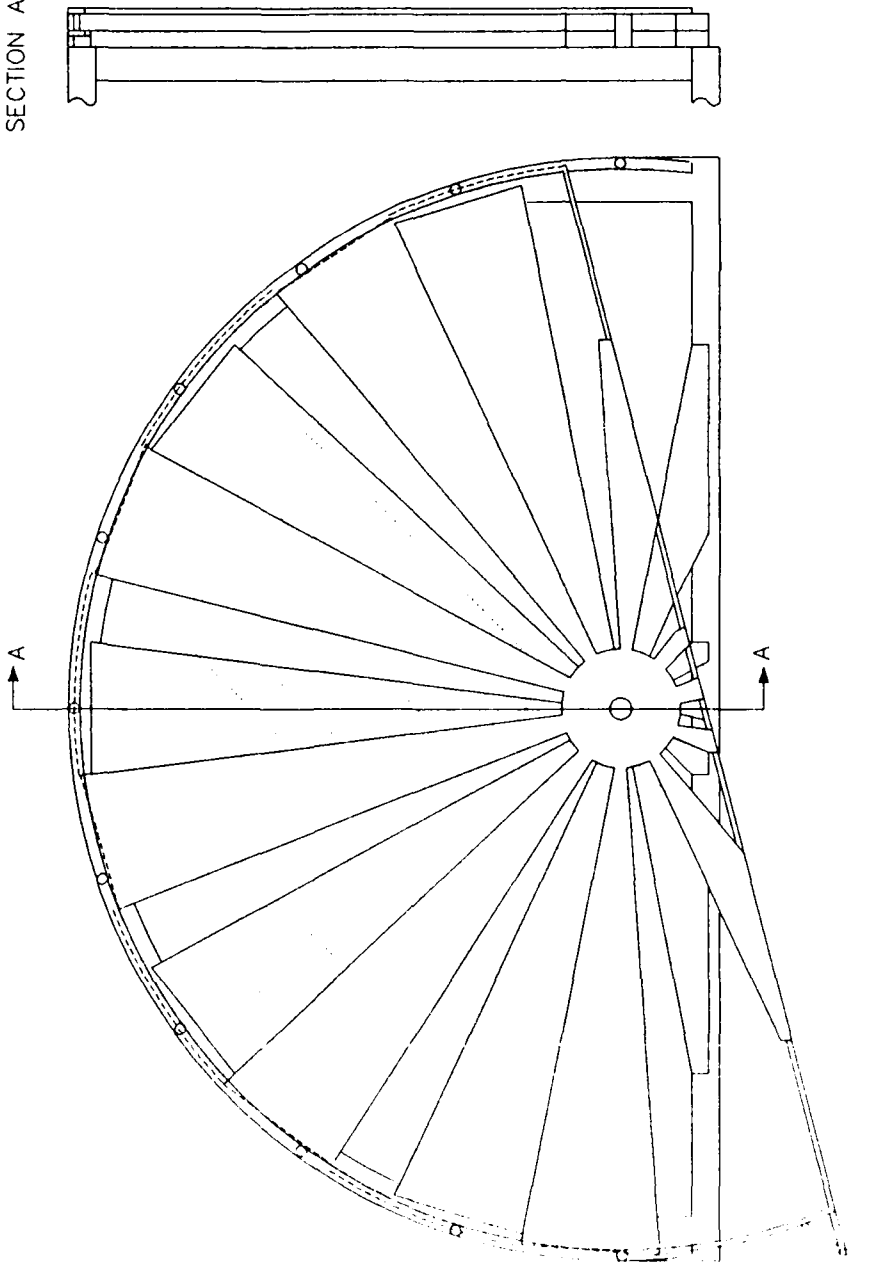


FIGURE 23 LB/TS REFLECTED WAVE ELIMINATOR STATOR/ROTOR DESIGN

23 illustrates the stator-rotor concept with the rotor rotated to block maximum area (minimum open area ratio).

The range of open area ratios obtainable with the stator-rotor concept is a function of the maximum open area ratio (1 - the area ratio always blocked by the stator) and the number of rotors selected for use in the RWE. Table 9 presents a summary of the range of open area ratios that can be achieved with up to four rotors. For the initial engineering analysis of the concept, a single rotor design with an open area ratio range of 20 to 60% was selected. The resulting design dimensions are given in Figures 21 and 22. As shown in Figure 22, the rotor elements are fastened at their tips to a circumferential frame to provide needed free end confinement.

TABLE 9. LB/TS EXIT PLANE OPEN-AREA RATIO RANGES FOR STATOR/ROTORS ACTIVE RWE DESIGNS

No. of Rotors	Stator Blocked	50	45	40	35	30	25	20	15	10	5
	Area Ratio (%)	50	55	60	65	70	75	80	85	90	95
1	Max. Open-Area Ratio (%)	0	10	20	30	40	50	60	70	80	90
2	Min. Open-Area Ratio (%)				0	10	25	40	55	70	85
3							0	20	40	60	80
4								0	25	50	75

To prevent rotor flutter from outflow or inflow at the exit plane, ball-type linear bearings would be mounted on both sides of the rotor outer circumference, rolling between two smooth circumferential tracks. Eleven equally spaced brackets, mounted to the LB/TS exit plane circumference, are used as the base for these two tracks. The rotor is driven circumferentially, through an attached lever, by an actuator rod which is operated by a hydraulic system similar to that used for the louver concept. As with the louvers design, the entire structure of the stator-rotor and the hydraulic system are mounted on a movable carriage to enable simple removal or operation.

The stator's ribs have a sloped front cover, facing the flow, to prevent stagnation-pressure conditions. All the ribs (stator and rotor) are hollow, to save weight. An assumed skin thickness of 2.5 cm was used to calculate the ribs' rectangular cross-section, found to be a depth of 30 cm, width varies from 25 cm at the origin up to about 240 cm at the end. The structure of stator and rotor was sized^{18,19} to withstand loads exerted by the flow^{20,21,22} for the case of 241 kPa/600 kT blast wave²³. In a trade-off among loads, weight and cost, the ribs of stator and rotor should be fabricated of ASTM A572-Grade 65 high-strength, low-alloy steel, which has a yield stress of 448 mPa²⁴.

The total weight of the stator-rotor design (carriage and hydraulic system excluded) is about 82555 kg, of which 42638 kg is weight of stator and static elements (11 brackets and 2 circumferential tracks) and 39916 kg belong to the weight of the rotor (including circumferential frame, bearings, lever and rod).

A polar moment-of-inertia was calculated for the stator-rotor RWE, and was found to be nearly 5000 times that of the rotating louver design. This amplitude was immediately seen as a major disadvantage for the stator-rotor concept, since the power requirement for rotation of the rotor is directly proportional to the polar moment-of-inertia. Further analysis of the stator-rotor RWE was suspended, because of the excessive power requirement calculated for the huge polar moment-of-inertia as compared to the other design options.

5.5 SIDE VENTING

The previously described computer modeling studies by UTIAS have resulted in the prediction of required open area ratios for the elimination of reflected waves for three different blast wave simulations in the LB/TS^{23,25}. The open area ratio to be generated by a RWE as a function of time is graphed in Figures 24 through 26 for the three low-yield cases. The data show that the range of open area ratio (fraction of total LB/TS cross-sectional area not blocked by the RWE)

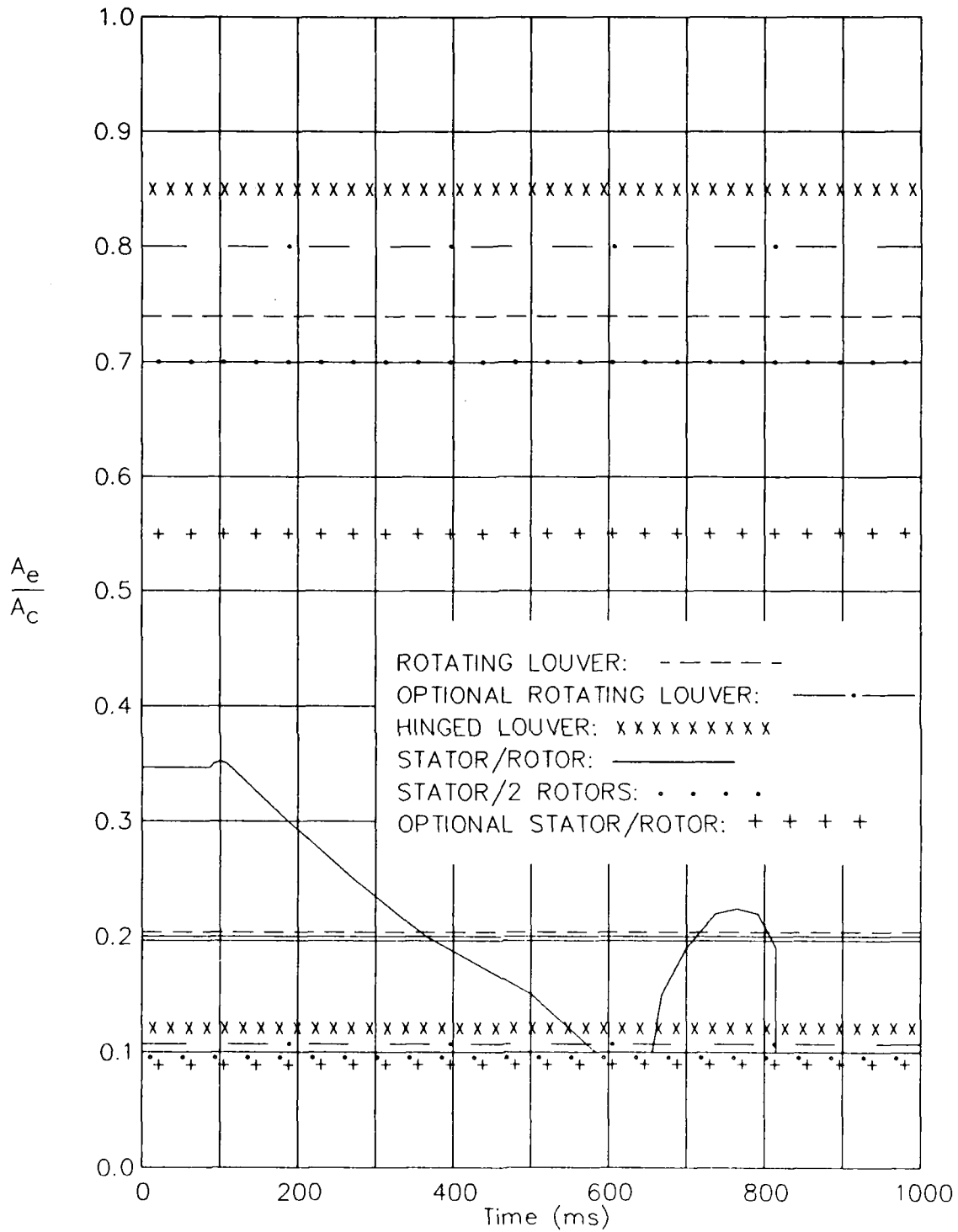


FIGURE 24: Area setting versus time for the active reflection eliminator used in the 13.8 kPa and low yield case.

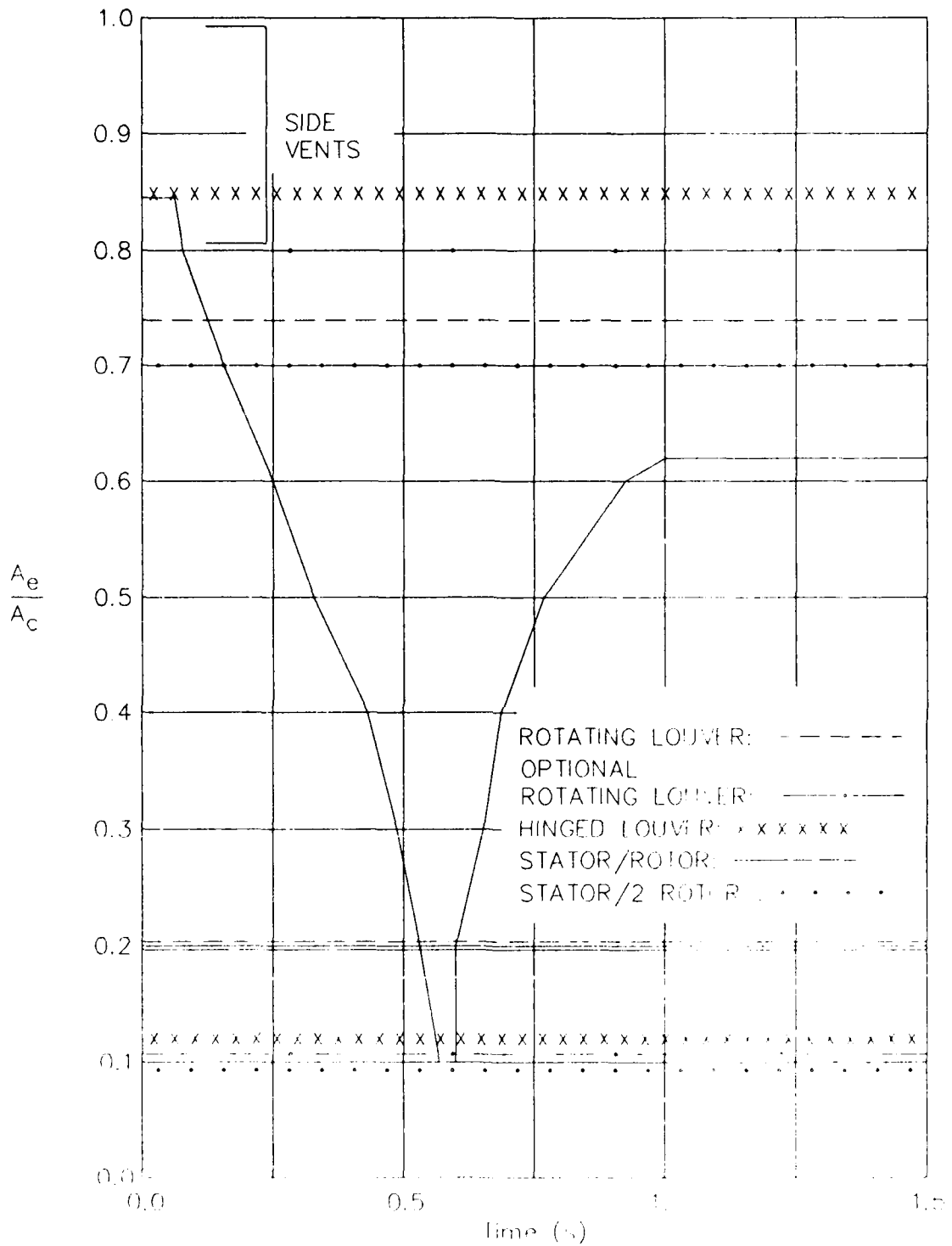


Figure 20c Area setting versus time for the reflector eliminator used in the 1000 ft/sec and low wind case.

needed for the simulation of the desired blast waves is greater than that provided by any of the designs previously described.

There are two approaches that can be employed to address this problem. The first is to simply "take what you can get," with a resulting overpressure profile that does not exactly simulate the blast wave of interest, and the second is to supplement the performance of the RWE mounted at the exit plane with an additional technique. Side venting provides a means to satisfy this second option. This concept uses vents in the side walls of the LB/TS near the exit. These vents may be active or passive, as discussed in the Introduction of this report. Analysis conducted under this effort indicates that the most effective use of side vents is in conjunction with an active RWE located at the exit plane of the LB/TS, rather than as the only means of reflected wave elimination.

The area ratios that can be achieved with the three RWE concepts presented in this report are depicted on the required open area ratio graphs of Figures 24 through 26. The graphs show that while additional open area is not required for the 13.8 kPa blast wave simulation, there is a need for additional venting for two of the three designs in the 103.4 kPa case. All designs require supplemental venting for the 241 kPa simulation. It must be noted that the UTIAS computer model arbitrarily cut off the minimum open area ratio at 10%, since perfect sealing of the LB/TS exit is not practical or desirable, especially while under dynamic loading.

The UTIAS quasi-steady model was used to study the effect of the upper limit on the open area ratio on the performance of a RWE in a simulated 241 kPa blast wave. For a maximum open area ratio of 85% in the RWE, the model predicted maximum overpressure 66% above the desired level. The forces calculated in Table 5 (column labeled "hydraulic force") reflect this condition, where for several of the early time steps the maximum open area was below the value required to accurately simulate the blast wave.

A second set of computations was also performed, where the RWE was assumed capable of providing the required open area ratio through contributions from an active RWE mounted on the open end of the LB/TS plus side vents (which may or may not be active). These data are presented in Table 10. It is quickly seen that the force requirement for the time zero condition has dropped by 40%, resulting in a more accurate desired overpressure profile which was provided by the increased range of the RWE/side vent combination. This result dramatically illustrates the value of side vents in an integrated RWE concept, which can accommodate the entire range of operation specified for the LB/TS.

Engineering of a conceptual design for side venting has not yet been undertaken but is recommended as a priority item now that side venting has been shown to be important to successful operation of an active RWE on the LB/TS. Initial analysis by UTIAS has shown that side vent area need be only about 5% greater than exit plane area for equivalent effect on the reflected wave. The modeling of side venting should also be examined in greater detail in the future.

TABLE 10. FORCE AND POWER REQUIREMENTS FOR ONE HINGED LOUVER (WITH PERFECT ELIMINATION OF THE RAREFACTION WAVE) FOR THE 241 kPa/10 kT CASE

Time (sec)	Area Ratio	Angle of Attack (deg) Theta	Angular Velocity (rad/sec) Omega	Angular Acceleration (rad/sec ²) Alpha	Inertia Power (KW)	Hydraulic Force (KN)	Hydraulic Power (KW)
0.0000	.850	4.82	0.00	0.00	0	80.02	0
.0150	.850	4.82	0.00	0.00	0	62.99	0
.0300	.850	4.82	0.00	0.00	0	50.40	0
.0450	.850	4.82	0.00	0.00	0	40.78	0
.0600	.833	6.00	1.38	91.74	.432	30.02	30.90
.0750	.770	10.47	5.20	255.08	4.835	28.82	97.90
.0900	.707	14.98	5.25	2.85	.060	20.28	68.22
.1050	.656	18.65	4.27	-65.10	-1.204	14.86	39.93
.1200	.608	22.24	4.18	-5.97	-.118	11.62	29.85
.1350	.561	25.81	4.15	-1.67	-.036	8.45	20.98
.1500	.515	29.42	4.21	3.66	.088	5.86	14.26
.1650	.470	33.11	4.29	5.22	.141	3.72	8.87
.1800	.425	36.90	4.41	8.49	.259	2.01	4.71
.1950	.381	40.86	4.60	12.59	.439	0.65	1.51
.2100	.337	45.04	4.86	17.28	.697	-0.37	-.85
.2250	.293	49.59	5.30	29.02	1.396	-1.06	-2.42
.2400	.247	54.76	6.02	47.90	2.868	-1.44	-3.33
.2550	.199	61.15	7.43	94.15	7.654	-1.33	-3.18
.2700	.143	70.69	11.10	244.50	33.033	0.18	.45
.2850	.100	84.80	16.42	354.70	70.760	10.83	10.70

6.0 CONCLUSIONS AND RECOMMENDATIONS

Analysis conducted by the UTIAS and reported in Section 4 presents a sound case for the recommendation of an active RWE configuration over a passive design. Simulations with the RCM computer model clearly show that passive RWEs for the LB/TS cannot simultaneously maintain peak pressure and positive phase duration for a given yield, especially at the high-yield end of the LB/TS operational envelope. The feasibility of an active RWE is confirmed in the engineering design analysis and power requirement computations discussed in this report. For the LB/TS envelope of interest, the flexibility and simulation capability of the active RWE designs become the paramount factor for their implementation.

The engineering studies indicate that the stator-rotor concept is the least desirable of the three investigated, because of its considerable mass and very large polar moment-of-inertia. Both the rotating louver and hinged louver concepts are promising, the rotating louver because of its minimal power requirement and the hinged louver because of its light weight. However, some design modification must be found to reduce the power requirement for the hinged louver before it can be considered clearly superior to the rotating louver concept. All active RWE concepts must be supplemented with active or passive side vents, to properly simulate the envelope of conditions specified for the LB/TS. It is recommended that the two louver concepts and side venting be further refined and analyzed for application to the LB/TS.

Future activities should address the growing need for experimental data with RWE concepts. A two-phase program is recommended, with the first phase testing to be done at 1/57th scale, and a second phase at 1/6th scale. The 1/57th scale testing is proof of the concept in nature, since it is not practical to actually scale the designs presented in this report for use on a 25.4 cm shock tube (the 1/57th scale test article). The 1/6th scale activities could be conducted in the 2.44 m shock tube at BRL. At this scale, the LB/TS designs could be scaled for performance testing of the components of an

RWE system. The existing active RWE concepts should be refined and analyzed in greater detail to obtain the information required to prepare scaled designs for testing. This effort should include additional modeling with UTIAS codes that are being upgraded, as well as more detailed design work on the RWE concepts themselves. A passive RWE should also be included in the scaled tests for comparison purposes. Hardware should be fabricated and installed on the BRL 25.4 cm shock tube for testing under actual shock conditions. Results of the scaled tests could be used to evaluate the active RWE performance and to validate the predictions made with the UTIAS computer model. In a second phase, design modifications suggested by the tests could be implemented and checked in a series of tests at 1/6th scale at BRL. This test series would be optional, pending the results of the smaller scale tests and the availability of the larger diameter shock tube for such a test program.

7.0 REFERENCES

1. Bowman, J.E. and G.B.F. Niblett, "The Passage of a Plane Shock Wave through a Wire Gauze," Proc. Phys. Soc., Lond. B, Vol. 68(12), 1008-1016, 1955.
2. Dosanjh, D.S., "Interaction of Grids with Travelling Shock Waves," NACA TN 3680, Sept. 1956.
3. Weidemann, A., "Study of Grids in Shock Tubes," Proc. of First Shock Tube Symposium, SWR-TM-57-2, Hq. AFSWC, Kirtland AFB, NM, 26-27 Feb. 1957.
4. Franks, W.J., "Interaction of a Shock Wave with a Wire Screen," UTIA Tech. Note No. 13, University of Toronto, May 1957.
5. Rudinger, G., "The Reflection of Shock Waves from an Orifice at the End of a Duct," Journal of Applied Math. and Physics, Vol. 96, 570-585, 1958.
6. Sadwin, L.d. and J. Berman, "Reflection and Rarefaction Elimination in Conical Shock Tubes," Proc. of Military Applications of Blast Simulators Symposium, Vol. 2, 582-591, DRES, Raiston, Alberta, Canada, July 1967.
7. Haverdings, W., "Evaluation of the 2.0-m Diameter Blast Simulator Driven by Fuel-Oxygen Explosives Charges," Proc. of Eighth International Symposium on Military Applications of Blast Simulation, Vol. I, I.1-1 to I.1-21, Spiez, Switzerland, 13-17 July 1983.
8. Clare, P.M. and R.D. Rowe, "The Foulness Multiton Air Blast Simulator. Part 1: Early Development the Gun Driven Facility," AWRE Report O31/74, Atomic Weapons Research Establishment, 1974.
9. Leys, I.C., "AWRE Foulness Nuclear Air Blast Simulator, Construction and Calibration of the Enlarged Facility," Proc. of Eighth International Symposium on Military Applications of Blast Simulation, Vol. II, I.1-1 to I.1-16, Spiez, Switzerland, 13-17 July 1983.
10. Languin, C., "Simulation de Choc et de Souffle. Compensateur d'Ondes de Detente de Bouche pour tube a Choc de 2400 mm de diametre de Veine. Description, Compte-Rendu de son Compartement Face aux Ondes de Souffle," Note Technique T-76-29, Centre d'Etudes de Gramat, Gramat, France.
11. Cadet, A. and J.B.G. Monzac, "Le Simulateur de Souffle a Grand Gabarit du Centre d'Etudes de Gramat: Description et Utilisation Operationelle," Proc. of Seventh International Symposium on Military Applications of Blast Simulation, Vol. I, I.2-1 to I.2-20, Medicine Hat, Canada, 13-17 July 1983.

12. Coulter, G.A., G. Bulmash and C.N. Kingery, "Experimental and Computational Modeling of Rarefaction Wave Eliminators Suitable for the BRL 2.44 m Shock Tube," BRL-TR-02503, U.S. Army Ballistics Research Laboratory, June 1983.
13. Kingery, C.N. and G.A. Coulter, "Rarefaction Wave Eliminator Concepts for a Large Blast/Thermal Simulator," BRL-TR-2634, U.S. Army Ballistic Research Laboratories, February 1985.
14. Gurevich, M.I., "Theory of Jets in Ideal Fluids," Academic Press, 1965.
15. Zhang, K.Y. and J.J. Gottlieb, "Simulation of a Blast Wave in a Shock Tube by Using Perforated Plates in the Driver," UTIAS Report No. 304, University of Toronto, March 1986.
16. Seventh International Symposium on Military Applications of Blast Simulation, Alberta, Canada, 13-17 July 1981, Proceedings, Vol. I.
17. Contract Progress Report on Active RWE-Engineering Conceptual Designs, Moshe Kuna, Denver Research Institute, University of Denver, January 1987.
18. Strength of Materials, John N. Cernica, Holt . . . , Inc., 1966.
19. Standard Handbook for Mechanical Engineers, Marks, 7th Ed.
20. Lecture Course Notes on Random-Choice Method, Prof. James Gottlieb, University of Toronto, May 1986.
21. Aerodynamics, L. J. Clancy, 1975, John Wiley & Sons, NY.
22. Compressible Fluid Flow, Michel A. Saad, Prentice-Hall, Inc., New Jersey, 1985.
23. Numerical Study of Reflection Eliminators, Prof. J.J. Gottlieb, University of Toronto, December 1986; Report to Denver Research Institute.
24. Manual of Steel Construction, 8th Ed., AISC, 10/81.
25. Fortran 77 Computer Program and Description of Its Use for Predicting the Area Setting of a Reflection Eliminator, Prof. J. J. Gottlieb, University of Toronto, January, 1987; Report to Denver Research Institute.
26. Aircraft Vibration and Flutter, C.R. Freberg and E.N. Kemler, John Wiley & Sons, Inc., New York, 1944.

APPENDIX :

SUPPLEMENTAL SIDE VENTING RAREFACTION WAVE ELIMINATOR

BRL PURCHASE ORDER #DAAD05-87-M-M469

INTENTIONALLY LEFT BLANK.

TABLE OF CONTENTS

1.	INTRODUCTION.....	A-3
2.	SIDE VENTING STEEL SHELL.....	A-3
2.1	Conceptual Design.....	A-3
2.2	Stress Analysis.....	A-6
3.	CLOSURE MECHANISMS.....	A-7
3.1	Venting-Area Closing Function.....	A-7
3.2	Sliding Cover Design.....	A-8
3.3	Rotating Louver Design.....	A-11
4.	CONCLUSIONS.....	A-12
	REFERENCES.....	A-13

INTENTIONALLY LEFT BLANK.

1. INTRODUCTION

The need for side vents in the Reflected Wave Eliminator (RWE) of the Large Blast and Thermal Simulator (LB/TS) has been documented in the preceding report. Computational results indicate that the maximum total open area requirement in the present operational envelope of the LB/TS is approximately equal to the cross sectional reference area of the LB/TS test section. The RWE designs investigated in the preceding study all require a support structure which obstructs at least 20% of the LB/TS cross sectional exit area, leaving at best 80% venting area. Therefore additional venting area is needed to meet the maximum open area requirement. A preliminary design for a supplementary side venting RWE is presented in this Appendix.

2. SIDE VENTING STEEL SHELL

The additional venting area can be located in the walls of the LB/TS expansion section near the tunnel exit. Analysis presented in Section 3.3 has shown that side venting is almost as effective as rear venting, even though the flow is parallel rather than perpendicular to the openings, as it is for the rear venting RWE. A total of 110% of the LB/TS cross-sectional area was required by the BRL for the end-venting RWE plus the side vents, based on anticipated flow loss of 10% (Kingery and Coulter, 1985). Since the most attractive RWE design provides a maximum of about 80% open area, the side vents must contribute the remaining 30%, or about 49 m² of open area that can be blocked during the passage of the simulated blast wave.

2.1 Conceptual Design

Steel was selected as the material most suitable for the side vent section, as the fabrication of a hemicylinder that is perforated with a series of holes is more effectively done in steel than in concrete. In particular, the holes cut for the side vents generate stress concentration points that would result in a significant increase in the thickness needed for a concrete section. A steel section could be fastened to the end of the concrete LB/TS structure as an extension of the expansion section with minimal modification to the design. The end mounted RWE would then be anchored to the steel side vent RWE section.

The number of vents employed is a compromise between a desire to use many small vents to minimize the effective stress concentration from the holes, and the conflicting need to minimize the number of vents in order to more economically mount and operate the closing mechanism. The open area provided by the side vents was kept to the minimum required for proper RWE operation over the LB/TS envelope.

The layout for the design is shown in Figures A-1 and A-2. The side view in Figure A-1 indicates three rows of vents located such that the vented area removes about 20% of the LB/TS shell structure in the side vent section. The vents are staggered for two reasons: first, this causes minimal flow disturbance on the downstream rows of vents from the row

SECTION C-C

NOTE: ALL DIMENSIONS ARE IN METERS

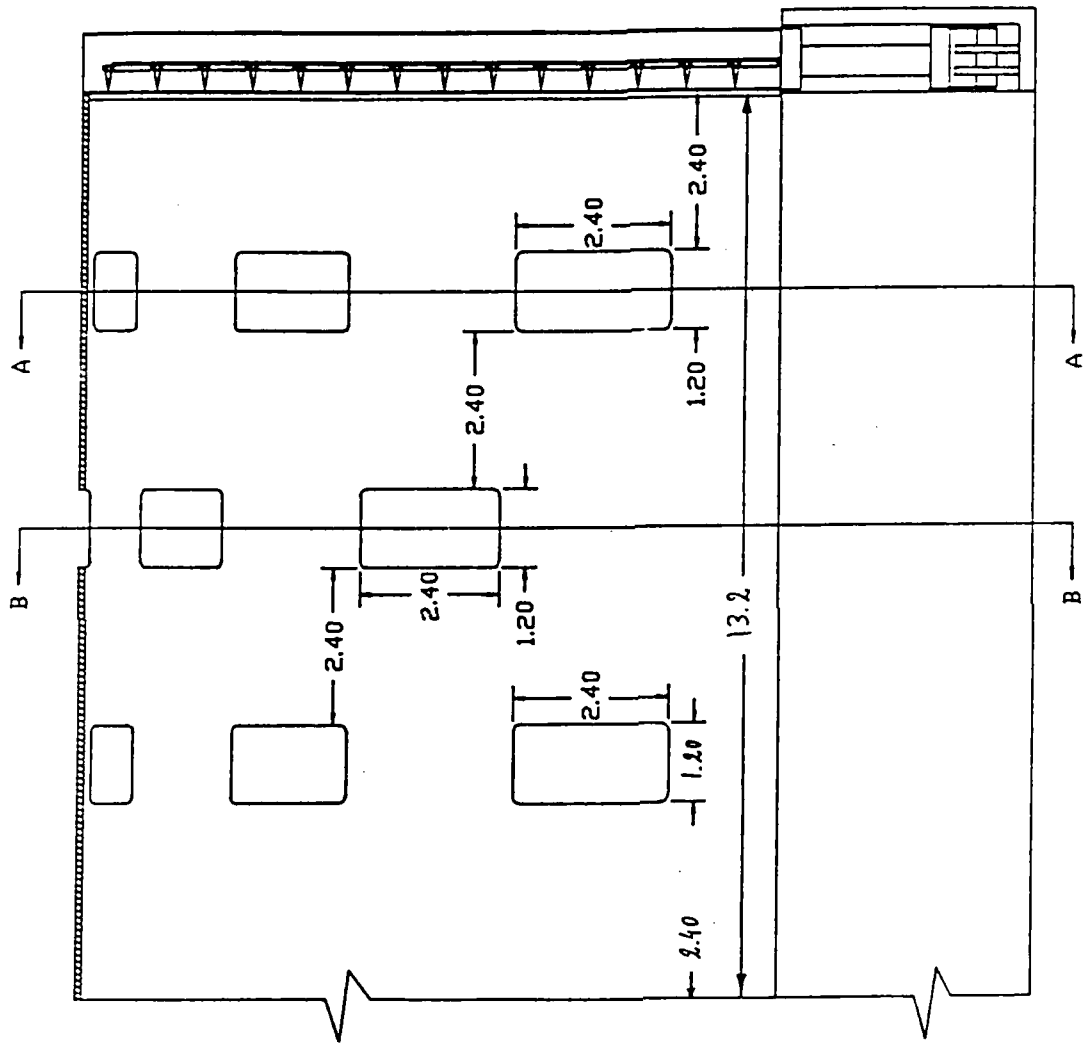


Figure A-1. LB/TS Exit Plane Cross Section Showing Location of Ports for Side Venting RWE

NOTE: ALL DIMENSIONS ARE IN METERS

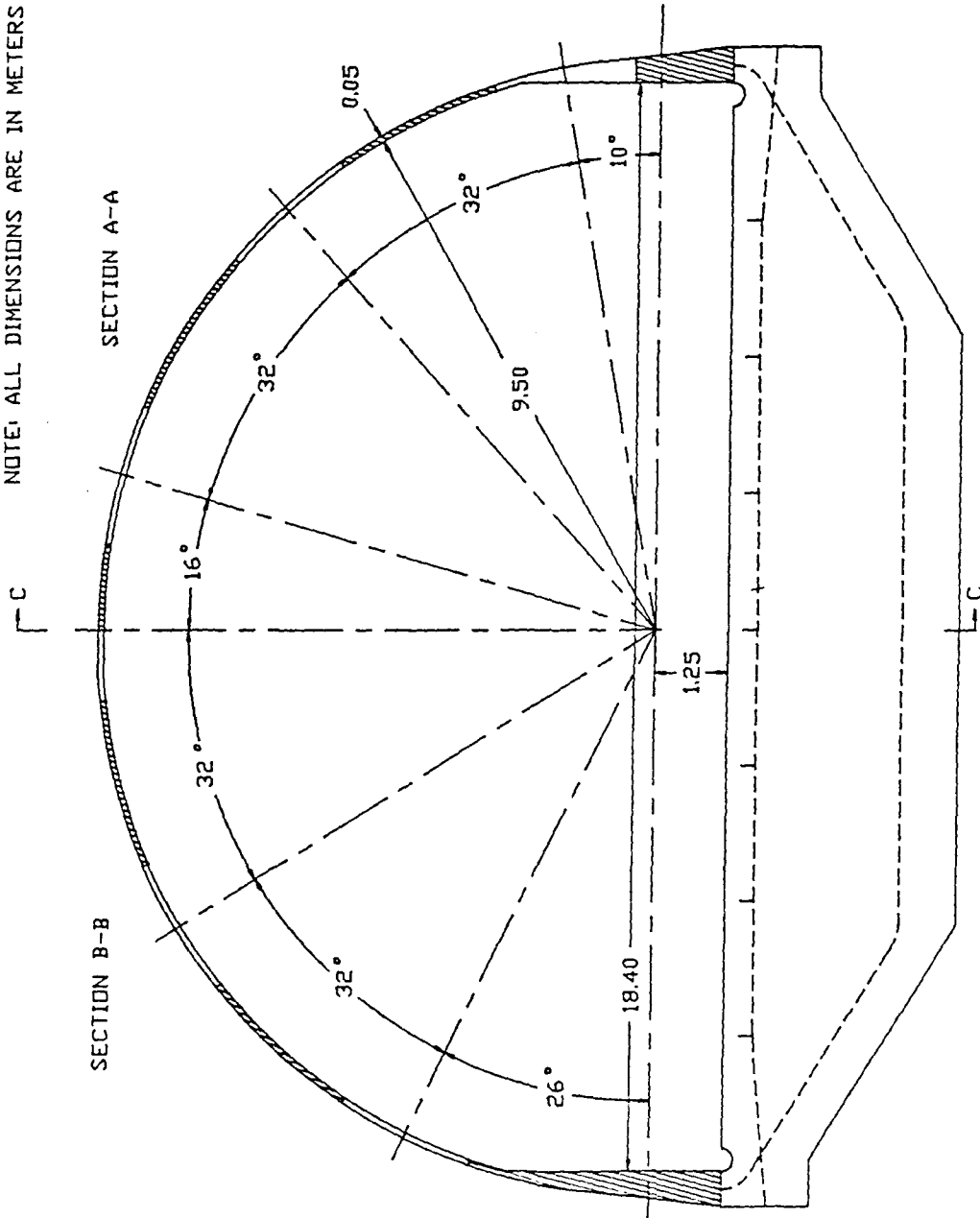


Figure A-2. Cross Section of LB/TS Through Ports of Side Venting RWE

immediately upstream; and second, the stress concentration in the side wall at the vent holes is minimized in this layout. The circumferential locations of the side vents in the two different row arrangements are presented in the opposite halves of the end view in Figure A-2.

2.2 Stress Analysis

The approach to the analysis of the loads generated in the steel side vent shell was modeled after an analysis presented in the 1959 text **Theory of Plates and Shells**, by S. Timoshenko. He notes that there are two kinds of stresses present in the (closed) hemicylinder: an axial stress along the cylinder (parallel to the direction of flow for a shock tube) and the circumferential, or hoop, stress. The hemicylinder is considered to be closed because the RWE is anchored to one end, and the driver section blocks the other. For such a configuration, the circumferential stress is twice the magnitude of the axial stress, and so becomes the controlling parameter.

Factors for calculating the local stress concentration as a function of spacing of the vents and fractional area removed were found in a paper from the Industrial Perforators Association, prepared by O'Donnell & Associates, Inc., Pittsburgh, PA, and confirmed by data from Marks' Handbook for Mechanical Engineers. This trade group sets standards for perforated metal from a number of manufacturers and used in a wide range of applications. The analysis shows that staggered rows of holes provide the greatest strength in the material to be perforated. Further, where the fraction of total surface area occupied by the holes is about 20%, the concentration of stress due to the holes in the plate material is about a factor of two. This value was then used in the design of the side vent section.

An exact solution to the stress in the side vent section would require a finite element computer model to be defined, run and analyzed. Such an effort is far beyond the scope of the effort undertaken here; however the approximations used are quite adequate for the preliminary design and feasibility analysis as presented.

In calculating the minimum yield to be used in the thickness computation, several additional factors were taken into account. First, a safety factor of 1.5 was applied to the 248 MPa (36,000 psi) yield of the ASTM A36 carbon steel selected as a baseline material. There is a significant spike at the leading edge of the shock reflected by the RWE that is short in duration, but for the 35 psi maximum static overpressure of the LB/TS operating envelope, this spike represents a peak about 1.8 times the nominal peak pressure. Thus the yield stress was reduced by an additional factor of 1.8. Finally, the holes in the side vent section cause a local concentration of stress, resulting in an adjustment to the yield stress by another factor of two. The total margin of safety is a factor of 5.4, resulting in a calculated material yield stress of 46.0 MPa (6,700 psi).

With all of the above factors taken into account along with the dimensions of the hemicylinder, a minimum thickness of 5 cm (2 in.) was calculated. The overall length of the steel side vent section is 13.2 m (43.3 ft), so that the weight of the section is 189,000 kg (2,080 tons).

This weight was used to estimate the cost of a steel side vent RWE. A unit cost of \$2 per pound of steel including fabrication and erection was used to arrive at an overall estimate. In addition, an estimate of \$100,000 was made for the rotating louvers and closure mechanism needed for the system, based on the calculated weight of the louvers and mechanism. The sum of the estimated costs for the side vent RWE was just under \$1,000,000.

The optimum aspect ratio for the vents was determined by consideration of the vent as removing material from the cross section of the steel shell over which the applied stress in both circumferential and axial directions could be carried. The aspect ratio was determined from the ratio of the hoop to axial stresses so as to equalize stresses in the LB/TS shell. Since the hoop stress is twice the axial stress, the vent ports should be twice as long in the circumferential direction as in the longitudinal. This yields the design presented in the earlier figures.

3. CLOSURE MECHANISMS

Three methods for closing the side vent ports were considered. Two of these employ linear motion of the closing cover and the third uses rotary motion. In the first method, a rectangular cover slides over each vent hole, moving in the direction of flow in the LB/TS from an upstream rest position on the steel wall. The second method also features a sliding motion, but in a circumferential direction, at a right angle to the direction of flow. The final method employs rotating louvers of the same dimensions as employed in the end-venting RWE. The louvers would be installed in pairs in the side vent hole, and would rotate about an axis through their center of gravity to block the vent.

An analysis was conducted to define the power requirements for motion of the side vent closure mechanisms. The sliding cover moving in the direction of flow was investigated, as was the rotating louvers concept. The circumferential sliding cover was not checked, because it was recognized to be a condition where much greater power would be required than for the longitudinal case. This is because of the orientation of the vent holes in the steel LB/TS section. The covers moving in the circumferential direction would have to move twice as fast to close the side vent open area. The power requirement has both a velocity and an acceleration component, so that the circumferential power requirement would be more than double that of the longitudinal sliding case.

3.1 Venting Area Closing Function

Two computer programs were used to calculate the needed vented area closing function for the early time in a 35 psi overpressure, 10 kT simulated blast wave. The 10 kT case was selected because it is of short duration and imposes rapid changes in open area ratio, which in turn requires maximum power to the closure mechanism. The DNA BLAST code was used to calculate the overpressure history shown in Figure A-3. In the short time span modeled, the blast wave has lost over two thirds of its initial overpressure. This rapid decay is significant because it necessitates rapid changes in open area ratio that are required to minimize the wave reflections at the LB/TS exit.

Next the calculated pressure history data were entered into the University of Toronto quasi-steady state ELIM code. This computer model calculates required RWE open area ratio settings as a function of the overpressure, the radius of rounding at the jet exit, a characteristic dimension (e.g., diameter) of the shock tube, and the ratio of specific heats for the gas used in the shock tube, assuming quasi-steady flow. The model results have been shown to be within 5% of predictions from the more sophisticated UTIAS Random Choice Model computer code, and are therefore useful for this conceptual design effort. Open area ratio requirements for two different radii of rounding at the vent port exit are shown in Figure A-4; the slight difference in open area ratio as a function of time is not significant in the calculation of louver power requirements discussed later.

The open area ratio data is used in a spreadsheet to calculate the changing open area requirements in the side vents as a function of time. This is an essential parameter for the computation of power requirements for operation of the side vent closure mechanisms.

3.2 Sliding Cover Design

In the two designs that slide in a linear motion, the cover is guided by a framework on the edge of the vent hole that prevents binding and provides a means to lubricate the motion so as to minimize friction. One possible way to handle the friction problem would be to attach wheels or bearings to the cover; however, simple lubrication of the sliding surfaces with grease may be adequate. The cover would be moved by a hydraulic linear actuator, controlled by a computer that monitors the parameters of the shock wave and adjusts the position of the cover to minimize the reflected wave in the LB/TS. Covers could be attached to a framework that would allow them to be moved in groups, perhaps with all vents in one of the staggered rows operated together.

The basic equation for the computation of the power requirements of the sliding vent cover is

$$P = F * v,$$

where P is the actuating power, F is the actuating force applied to the moving cover and v is the velocity at which the cover moves. Thus the most rapid changes in open area ratio will require the greatest velocities and maximum power. The actuating force was assumed to consist of two components: the inertial force, equal to the mass of the cover times the acceleration which it is experiencing, and the friction force resisting the motion of the cover.

The friction force was assumed to be generated when the interior overpressure pressed the cover back against the framework that guides its motion. Depending on the location of the individual vent hole on the circumference of the hemicylindrical shell of the LB/TS, the weight of the cover may counteract or increase the friction force. The friction force was found to be less than 10% of the total force for all cases run, so that neglecting the cover weight in the calculation of friction force was believed to be a justified simplification. The model was set up on a personal computer spreadsheet, so that results for a number of input conditions could be calculated.

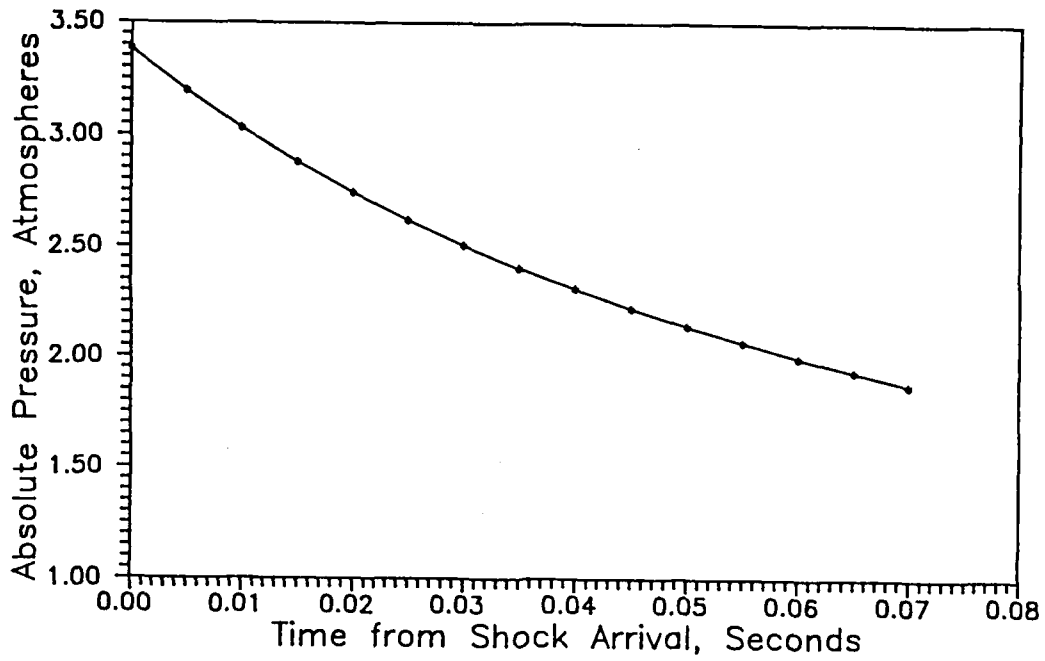


Figure A-3. Overpressure Waveform for LB/TS Simulation

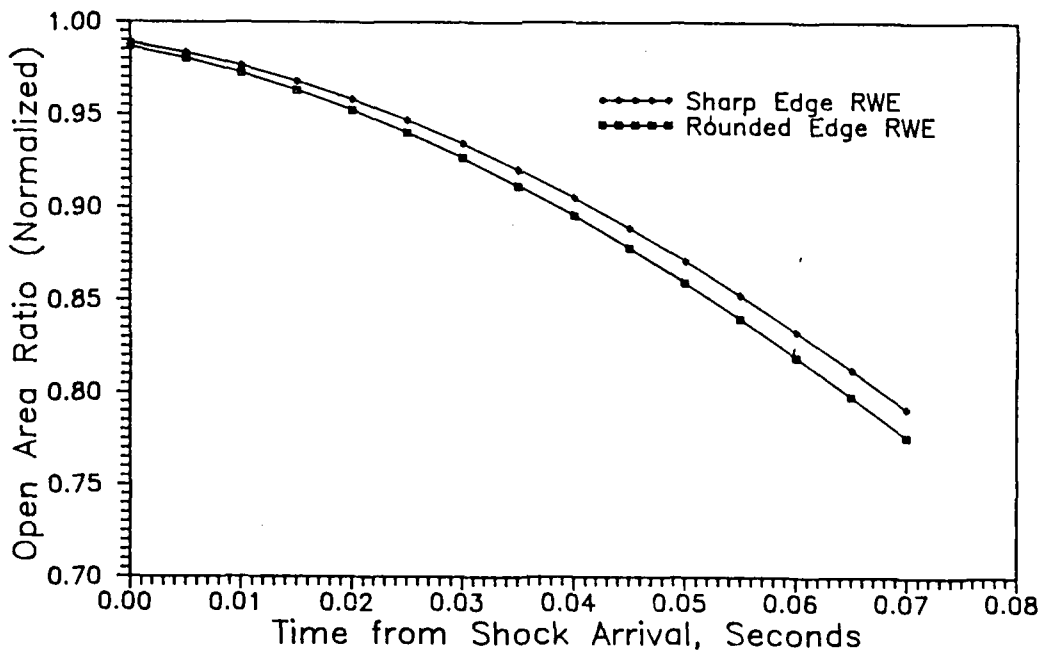


Figure A-4. Calculated Open Area Ratio Setting for RWE

The spreadsheet used a simple differencing scheme to compute closure velocity and acceleration, where the values for each time step were calculated as the change in position or velocity divided by the change in time for velocity or acceleration, respectively. Time steps of five milliseconds were selected to provide adequate resolution in the differencing operation, and the simulated waveform (and corresponding changing RWE open area ratio) was carried through to the time when the side vents would be fully closed, and only the end vents operating. It should also be noted that the power required to stop the vent covers at the end of their travel was not considered; a mechanical damper-type stop is one alternative.

Results of the spreadsheet calculations are summarized in Table A-1. The total open area ratio and fraction of that total generated by the side vents area shown for the times listed in the first column. The power requirements for a single cover are presented for three different cases, which differ in the mass assumed for the side vent cover and the factor assumed for the coefficient of friction between the cover and the frame that guides its motion. Total power requirements would thus be 17 times the single cover values given here.

TABLE A-1. CALCULATED POWER REQUIREMENTS FOR SLIDING SIDE VENT COVERS

Time (sec)	Total Open Area Ratio	Side Vent Area Ratio	Required Power (kW)		
			Case 1	Case 2	Case 3
0.000	0.9888	0.1888	0	0	0
0.005	0.9831	0.1831	4,837	1,210	1,833
0.010	0.9761	0.1761	1,417	318	493
0.015	0.9677	0.1677	1,819	409	634
0.020	0.9579	0.1579	2,122	477	740
0.025	0.9467	0.1467	2,425	544	846
0.030	0.9342	0.1342	2,528	568	880
0.035	0.9202	0.1202	3,236	726	1,129
0.040	0.9051	0.1051	2,625	591	910
0.045	0.8887	0.0887	3,326	747	1,157
0.050	0.8713	0.0713	2,781	627	960
0.055	0.8527	0.0527	3,512	790	1,218
0.060	0.8331	0.0331	3,140	708	1,084
0.065	0.8127	0.0127	2,685	607	920
0.070	0.7915	0.0000	-18,558	-3,075	-4,951

In Case 1 a solid steel cover of 5 cm thickness is assumed. This yields a total cover mass of 1,123 kg. In addition, a sliding friction factor of 0.08 is used, representing a lubricated steel on steel configuration. This is thus a "worst case" condition, where all parameter values are selected to produce a maximum power requirement. The table shows that about 3,500 kilowatts are needed to move this cover, and that there is little variation over the 85 milliseconds that the side vents are active. Larger values appearing at the start and near the end of the motion are artifacts of the differencing scheme used to calculate the velocities and accelerations, and may be ignored.

As a second case, a more sophisticated design structure with reinforcing ribs was defined to reduce the mass necessary to withstand the overpressure of the simulated blast wave. Also the friction factor was reduced to 0.02 to represent an improved cover mount with rollers in the frame. These design changes resulted in a peak power requirement of 790 kW, which represents a reduction from Case 1 of 77%.

The third case assumes an intermediate mass of the cover equal to 400 kg. Again the friction factor is assumed to be 0.02. The results for Case 3 presented in Table 1 show a peak power requirement of about 1,200 kilowatts.

The significant mass of the cover in cases 1 and 3 make an important contribution to the significant power requirements predicted for the sliding cover configuration; recall that the calculations represent a single cover. A review of these results indicate that the rotating louver alternative should be evaluated, and also that a design where the sliding cover moves twice as far (to cover the vent in a circumferential rotation) is not feasible.

3.3 Rotating Louver Design

The rotating louvers are operated in the same way as in the end-venting RWE, with a hydraulic actuator providing the needed power. This actuator can be either directly rotary or linear, with a lever arm to convert the motion to rotary at the louver pivot. There is a slight change in dimensions of the vent ports as shown in Figure 1 to accommodate the length and width of the louvers used in the RWE, which are 2.03 m by 0.67 m. In addition, the louvers block 10% of the vent area in the fully open position; thus the requirement for open area equal to 30% of the LB/TS cross section is met with the addition of three more vents, for a total of twenty in this configuration. The advantages of using a standardized louver size in both the end and side vent RWEs is worth the small change in the side vent layout (most likely an additional staggered row). Two louvers are mounted in each side vent with their axes of rotation in the circumferential direction on the steel LB/TS shell.

Since the side venting louvers have the same basic dimensions as the louvers of the end-venting RWE, it was easy to modify the BASIC computer model written to calculate the power requirements for the rotating louver RWE to perform a similar function on the side vent rotating louvers. Since the motion of the louver is rotary in this design, the equation used to calculate the required power is:

$$P = T * \text{Omega}$$

where P is the required power, T is the applied torque and Omega is the angular velocity. The applied torque T is product of the polar moment of inertia of the louver times the angular acceleration, alpha. As before, a differencing scheme was used to compute values for alpha and omega for use in the power calculation.

Output from the computer model is presented in Table A-2. It is obvious that the power requirements are much diminished compared to the sliding cover cases. In fact, the power requirements remain an order of magnitude below the sliding cover levels (two louvers are needed for each side vent) until late in the time period examined. The dramatic jump in power at 60 milliseconds occurs as the louver approaches the fully closed

position, because the change in open area is not linear with rotary position of the louver, but rather a sine function. This problem is easily solved by allowing the end louvers to begin to close before the side vents are fully closed, thus providing a further reduction in the total open area in addition to the rapidly closing side vents. It is therefore advantageous to propose a rotating louver system for the side vents with a maximum applied power of 35 kW per louver, or 1,400 total kW for a 20 port side venting system. This compares with a minimum requirement of 750 kW per side vent for the sliding cover design.

TABLE A-2. POWER REQUIREMENT FOR A SINGLE ROTATING LOUVER IN A SIDE VENT

Time (sec)	Side Vent Area Ratio	Angular Position (degrees)	Angular Velocity (rad/sec)	Angular Acceleration (rad/sec ²)	Required Power (kW)
0.000	0.1888	27.79	0.00	0.00	0.000
0.005	0.1831	28.84	3.66	732	10.2
0.010	0.1761	30.14	4.55	177	3.1
0.015	0.1677	31.73	5.54	198	4.2
0.020	0.1579	33.61	6.58	209	5.2
0.025	0.1467	35.82	7.70	224	6.6
0.030	0.1342	38.36	8.86	231	7.8
0.035	0.1202	41.31	10.31	289	11.4
0.040	0.1051	44.65	11.67	273	12.2
0.045	0.0887	48.52	13.49	365	18.8
0.050	0.0713	52.97	15.55	411	24.5
0.055	0.0527	58.31	18.64	618	44.0
0.060	0.0331	65.00	23.35	943	84.1
0.065	0.0127	74.58	33.42	2,014	257.0
0.070	0.0000	89.17	50.93	3,501	680.8

4. CONCLUSIONS

This letter report presents a preliminary design for side vents that would provide adequate RWE open areas to cover the operating envelope of the LB/TS. The recommended closing mechanism for the side vents is a rotating louver of the same design as used in the end-venting RWE. The rotating louver possesses several advantages over the sliding cover, including greatly reduced power and minimal cost.

Based on the review of cited references and the earlier design work for the end-venting RWE, a set of design requirements emerged that guided the development of the configuration shown earlier. These included:

- o The side vents have only the minimum area required to supplement the end-venting RWE. This is important because the steel shell is an addition to the LB/TS and its cost is minimized when its length is minimized.
- o The side vents should be numerous and small rather than few and large. There is an obvious tradeoff here in that closure mechanisms must be designed and built for each vent, yet very large vents cause a disproportionately greater concentration in the stress, especially if the vents are close together and there is insufficient cross sectional area between the vents to carry the load.
- o The side vents should be rectangular rather than square and have their length perpendicular to the LB/TS axis of flow, for reasons described above.
- o The vents should have rounded corners, to minimize the stress concentration due to the removal of material from the wall of the steel section.
- o The rows of side vents should be staggered with adequate separation, to allow sufficient cross sectional area to carry the stresses.

The impact of side vents on the shape of the reflected wave generated by the RWE is unknown at this time, and is being investigated with a computer model by researchers at the University of Toronto Institute for Aerospace Studies. It is also recommended that side vents be simulated during scaled tests of the RWE concept scheduled to be run on the BRL 10 inch shock tube in the summer of 1988. Perhaps the simplest manner to simulate the side vents is to space the model RWE a short distance off the end of the test shock tube, allowing an open area between the end flange and the frame for the model RWE.

REFERENCES

- Gottlieb, J. J., FORTTRAN 77 Computer Program and Description of Its Use for Predicting the Area Setting of a Reflection Eliminator, University of Toronto Institute for Aerospace Studies, Toronto, Ontario, Jan 1987.
- Kingery, C. N. and G. A. Coulter, Rarefaction Wave Eliminator Concepts for a Large Blast/Thermal Simulator, BRL Technical Report No. BRL-TR-2634, US Army Ballistic Research Laboratory, Aberdeen Proving Ground, MD, February, 1985.
- Marks' Standard Handbook for Mechanical Engineers**, 7th edition, McGraw Hill, New York, 1967.
- Strength of Materials Perforated with Round Holes in a Standard Staggered Pattern, O'Donnell & Associates report for the Industrial Perforators Association, ODAI-1448-1-81, May, 1981.
- Timoshenko, S., **Theory of Plates and Shells**, McGraw Hill, New York, 1959.

INTENTIONALLY LEFT BLANK.

<u>No of</u>	<u>Organization</u>	<u>No of</u>	<u>Organization</u>
<u>Copies</u>		<u>Copies</u>	
1	Office of the Secretary of Defense OUSD(A) Director, Live Fire Testing ATTN: James F. O'Bryon Washington, DC 20301-3110	1	Director US Army Aviation Research and Technology Activity Ames Research Center Moffett Field, CA 94035-1099
(Unclass., unlimited) 12	Administrator	1	Commander
(Unclass., limited) 2	Defense Technical Info Center		US Army Missile Command
(Classified) 2	ATTN: DTIC-DDA Cameron Station Alexandria, VA 22304-6145		ATTN: AMSMI-RD-CS-R (DOC) Redstone Arsenal, AL 35898-5010
1	HQDA (SARD-TR) WASH DC 20310-0001	1	Commander US Army Tank-Automotive Command ATTN: AMSTA-TSL (Technical Library) Warren, MI 48397-5000
1	Commander US Army Materiel Command ATTN: AMCDRA-ST 5001 Eisenhower Avenue Alexandria, VA 22333-0001	1	Director US Army TRADOC Analysis Command ATTN: ATAA-SL White Sands Missile Range, NM 88002-5502
1	Commander US Army Laboratory Command ATTN: AMSLC-DL Adelphi, MD 20783-1145	(Class. only) 1	Commandant US Army Infantry School ATTN: ATSH-CD (Security Mgr.) Fort Benning, GA 31905-5660
2	Commander Armament RD&E Center US Army AMCCOM ATTN: SMCAR-MSI Picatinny Arsenal, NJ 07806-5000	(Unclass. only) 1	Commandant US Army Infantry School ATTN: ATSH-CD-CSO-OR Fort Benning, GA 31905-5660
2	Commander Armament RD&E Center US Army AMCCOM ATTN: SMCAR-TDC Picatinny Arsenal, NJ 07806-5000	1	Air Force Armament Laboratory ATTN: AFATL/DLODL Eglin AFB, FL 32542-5000 <u>Aberdeen Proving Ground</u>
1	Director Benet Weapons Laboratory Armament RD&E Center US Army AMCCOM ATTN: SMCAR-CCB-TL Watervliet, NY 12189-4050	2	Dir, USAMSAA ATTN: AMXSY-D AMXSY-MP, H. Cohen
1	Commander US Army Armament, Munitions and Chemical Command ATTN: SMCAR-ESP-L Rock Island, IL 61299-5000	1	Cdr, USATECOM ATTN: AMSTE-TO-F
1	Commander US Army Armament, Munitions and Chemical Command ATTN: SMCAR-ESP-L Rock Island, IL 61299-5000	3	Cdr, CRDEC, AMCCOM ATTN: SMCCR-RSP-A SMCCR-MU SMCCR-MSI
1	Commander US Army Armament, Munitions and Chemical Command ATTN: SMCAR-ESP-L Rock Island, IL 61299-5000	1	Dir, VLAMO ATTN: AMSLC-VL-D
1	Commander US Army Aviation Systems Command ATTN: AMSAV-DACL 4300 Goodfellow Blvd. St. Louis, MO 63120-1798		

<u>No. of Copies</u>	<u>Organization</u>	<u>No. of Copies</u>	<u>Organization</u>
1	Director of Defense Research and Engineering ATTN: DD/TWP Washington, DC 20301	1	Commander US Army Foreign Science and Technology Center ATTN: Research and Data Branch 220 7th Street, NE. Charlottesville, VA 22901
1	Assistant Secretary of Defense (Atomic Energy) ATTN: Document Control Washington, DC 20301	1	Commander US Army Logistics Management Center ATTN: ATCL- O (R. Cameron) Fort Lee, VA 23801
1	Director Defense Advanced Research Projects Agency ATTN: Tech Lib 1400 Wilson Boulevard Arlington, VA 22209	1	Commander US Army Materials Technology Laboratory ATTN: SLCMT-ATL Watertown, MA 02172-0001
2	Director Federal Emergency Management Agency ATTN: Public Relations Office Technical Library Washington, DC 20472	1	Commander US Army Strategic Defense Command ATTN: CSSD-H-MPL (Tech Lib) CSSD-H-XM (Dr. Davies) P.O. Box 1500 Huntsville, AL 35807
6	Director Defense Nuclear Agency ATTN: CSTI (Tech Lib) DDIR DFSP (Ullrich) NANS OPNA SPSD (Goering/Rohr) TDTR (Kennedy/Hrinishin) Washington, DC 20305	1	Commander US Army Engineer Division ATTN: HNDED-FD P.O. Box 1500 Huntsville, AL 35807
3	Commander Field Command, DNA ATTN: FCPR FCTMOF NMHE/CDR Lund Kirkland AFB, NM 87115	3	Commander US Army Corps of Engineers Waterways Experiment Station ATTN: CAWES-SS-R (J. Watt) CAWES-SE-R (J. Ingram) CAWES-TL (Tech Lib) P.O. Box 631 Vicksburg, MS 39180-0631
3	Director US Army Harry Diamond Labs ATTN: SLCHD-NW-RA (L. Bellivcau) SLCHD-NW-P (Gwaltney/Meszaros) SLCHD-TA-L (Tech Lib) 2800 Powder Mill Road Adelphi, MD 20783-1145	1	Commander US Army Research Office ATTN: SLCRO-D P.O. Box 12211 Research Triangle Park, NC 27709-2211
1	Commander, USACECOM R&D Technical Library ATTN: ASQNC-ELC-I-T, Myers Center Fort Monmouth, NJ 07703-5301	1	Director HQ, TRADOC RPD ATTN: ATRC-RPR (Mr. Radda) Fort Monroe, VA 23651-5143
1	Director US Army Missile and Space Intelligence Center ATTN: AIAMS-YDL Redstone Arsenal, AL 35898-5500	1	Director TRAC-WSMR ATTN: ATRC-WC (Mr. Kirby) White Sands Missile Range, NM 88002-5502

<u>No. of Copies</u>	<u>Organization</u>	<u>No. of Copies</u>	<u>Organization</u>
1	Director US Army TRADOC Center ATTN: ATRC Fort Leavenworth, KS 66027-5200	1	Commanding Officer White Oak Warfare Center ATTN: Code WA501 (NNPO) Silver Spring, MD 20902-5000
1	Commander US Army Test and Evaluation Command Nuclear Effects Laboratory ATTN: STEWS-TE-NO (Dr. J.L. Meason) P.O. Box 477 White Sands Missile Range, NM 88002	1	Commander Naval Weapons Center ATTN: Code 533 (Tech Library) China Lake, CA 93555-6001
1	Commandant Interservice Nuclear Weapons School ATTNL Technical Library Kirtland AFB, NM 87115	1	Commander Naval Weapons Evaluation Facility ATTN: Document Control Kirtland AFB, NM 87117
1	Chief of Naval Research ATTN: N. Perrone Department of the Navy Arlington, VA 22217	1	Commander Naval Research Laboratory ATTN: Code 2027, Tech Library Washington, DC 20375
1	Commander Naval Facilities Engineering Command ATTN: Technical Library Washington, DC 20360	1	Superintendent Naval Postgraduate School ATTN: Code 2124, Tech Library Monterey, CA 93940
5	Officer-in-Charge Naval Construction Battalion Center Civil Engineering Laboratory ATTN: Code L64 (N. P. Clark) Code L54 (R. J. Odello) Code L51 (W. Keenan) Code L06C/L08A (Tech Lib) Port Huene, CA 93041	1	AFSC/SDOA Andrews AFB, MD 20334
1	Commander David W. Taylor Naval Ship Research and Development Command ATTN: Code 522 (Lib Div) Bethesda, MD 20084-5000	2	Air Force Armament Laboratory ATTN: AFATL/DOIL AFATL/DLYV Englin AFB, FL 32542-5000
1	Commander Naval Surface Warfare Center ATTN: Code DX-21 (Library) Dahlgren, VA 22448-5000	1	AFESC/RDCS ATTN: Paul Rosengren Tyndall AFB, FL 32403
1	Officer in Charge White Oak Warfare Center Detachment ATTN: Code E232 (Tech Library) 10901 New Hampshire Ave. Silver Spring, MD 20903-5000	1	RADC (EMTLD/Docu Library) Griffiss AFB, NY 13441
		3	Air Force Weapons Laboratory ATTN: NTE NTED NTES Kirtland AFB, NM 87117-6008
		1	AFIT ATTN: Tech Lib (Bldg. 640/B) Wright-Patterson AFB, OH 45433
		1	FTD/NIIS Wright-Patterson AFB Ohio 45433
		1	Director Lawrence Livermore Lab ATTN: Tech Info Dept L-3 P.O. Box 808 Livermore, CA 94550

<u>No. of Copies</u>	<u>Organization</u>	<u>No. of Copies</u>	<u>Organization</u>
2	Director Los Alamos Scientific Lab. ATTN: Mr. Th. Dowler, MS-F602 Doc Control for Reports Library P.O. Box 1663 Los Alamos, NM 87545	1	EATON Corporation Defense Valve and Actuator Div. ATTN: Mr. J Wada 2338 Alaska Ave. El Segundo, CA 90245-4896
3	Director Sandia Laboratories ATTN: Doc Control 3141 Mr. C. Cameron, Div 6251 Mr. A. Chabai, Div 7112 P.O. Box 5800 Albuquerque, NM 87185-5800	1	Kaman Sciences Corporation ATTN: Mr. F. W. Balicki 6400 Uptown Boulevard N.E. Suite 300 Albuquerque, NM 87110
1	Director Sandia Laboratories Livermore Laboratory ATTN: Doc Control for Tech Library P.O. Box 969 Livermore, CA 94550	2	R&D Associates ATTN: Technical Library Dr. Allan Kuhl P.O. Box 9695 Marina Del Rey, CA 90291
1	Director National Aeronautics and Space Administration ATTN: Scientific and Tech Info Fac P.O. Box 8757, BWI Airport Baltimore, MD 21240	1	Science Applications International Corp. ATTN: Mr J. Guest 2109 Air Park Rd SE Albuquerque, NM 87106
1	Director NASA-Langley Research Center ATTN: Tech Lib Hampton, BA 23665	1	Sparta, Inc. Los Angeles Operations ATTN: I. B. Osofsky 3440 Carson Street Torrance, CA 90503
2	Applied Research Associates, Inc. ATTN: N. H. Ethridge J. Keefer P.O. Box 548 30 Diamond St. Aberdeen, MD 21001	1	Sverdrup Technology, Inc. ATTN: R. F. Starr P.O. Box 884 Tullahoma, TN 37388
1	Applied Research Associates, Inc. ATTN: R. L. Guice 7114 West Jefferson Ave., Suite 305 Lakewood. CO 80235	2	S-CUBED ATTN: C. E. Needham Lynn Kennedy 2501 Yale Blvd. SE Albuquerque, NM 87106
1	Black and Veatch, Engineers- Architects ATTN: H. D. Laverentz 1500 Meadow Lake Parkway Kansas City, MO 64114	3	S-CUBED ATTN: Technical Library R. Duff K. Pyatt P.O. Box 1620 La Jolla, CA 92037-1620
1	Dynamics Technology, Inc. ATTN: D. T. Hove Suite 300 21311 Hawthorne Blvd. Torrance, CA 90503	1	Battelle Memorial Institute ATTN: Technical Library 505 King Avenue Columbus, OH 43201
		2	Denver Research Institute University of Denver ATTN: Mr. J. Wisotski Technical Library P.O. Box 10127 Denver, CO 80210

No. of
Copies

Organization

- 1 Massachusetts Institute of
Technology
ATTN: Technical Library
Cambridge, MA 02139

- 2 New Mexico Engineering Research
Institute (CERF)
University of New Mexico
ATTN: Dr. J. Leigh
Dr. R. Newell
P.O. Box 25
Albuquerque, NM 87131

Aberdeen Proving Ground

Cdr, USATECOM
ATTN: AMSTE-TE-F (L. Telcetski)

Cdr, USATHMA
ATTN: AMXTH-TE

INTENTIONALLY LEFT BLANK.

USER EVALUATION SHEET/CHANGE OF ADDRESS

This Laboratory undertakes a continuing effort to improve the quality of the reports it publishes. Your comments/answers to the items/questions below will aid us in our efforts.

1. BRL Report Number BRL-CR-628 Date of Report MARCH 1990

2. Date Report Received _____

3. Does this report satisfy a need? (Comment on purpose, related project, or other area of interest for which the report will be used.) _____

4. Specifically, how is the report being used? (Information source, design data, procedure, source of ideas, etc.) _____

5. Has the information in this report led to any quantitative savings as far as man-hours or dollars saved, operating costs avoided, or efficiencies achieved, etc? If so, please elaborate. _____

6. General Comments. What do you think should be changed to improve future reports? (Indicate changes to organization, technical content, format, etc.) _____

CURRENT
ADDRESS

Name

Organization

Address

City, State, Zip Code

If indicating a Change of Address or Address Correction, please provide the New or Correct Address in Block 6 above and the Old or Incorrect address below.

OLD
ADDRESS

Name

Organization

Address

City, State, Zip Code

-----FOLD HERE-----

DEPARTMENT OF THE ARMY

Director
U.S. Army Ballistic Research Laboratory
ATTN: SLCBR-DD-T
Aberdeen Proving Ground, MD 21005-5066
OFFICIAL BUSINESS



**NO POSTAGE
NECESSARY
IF MAILED
IN THE
UNITED STATES**

BUSINESS REPLY MAIL
FIRST CLASS PERMIT No 0001, APG, MD

POSTAGE WILL BE PAID BY ADDRESSEE

Director
U.S. Army Ballistic Research Laboratory
ATTN: SLCBR-DD-T
Aberdeen Proving Ground, MD 21005 9989



-----FOLD HERE-----